FINITE DIFFERENCE METHODS FOR THE SHALLOW WATER EQUATIONS ON VARIOUS HORIZONTAL GRIDS

Zaviša I. Janjić
Federal Hydrometeorological Institute
Belgrade, Yugoslavia
and
Fedor Mesinger
Department of Physics and Meteorology
Belgrade University, Belgrade, Yugoslavia

CONTENTS

1. INTRODUCTION

Horizontal differencing is one of the major problems in designing finite-difference numerical models of the atmosphere. In order to examine this problem in more detail, it is convenient to start from the shallow water equations

$$\frac{\partial u}{\partial t} + \mathbf{v}\cdot\nabla u + g\frac{\partial h}{\partial x} - fv = 0\,, \quad \frac{\partial v}{\partial t} + \mathbf{v}\cdot\nabla v + g\frac{\partial h}{\partial y} + fu = 0\,, \qquad (1.1)$$

$$\frac{\partial h}{\partial t} + \nabla\cdot h\mathbf{v} = 0\,.$$

Here, u and v are velocity components, $\mathbf{v}$ is the wind vector and h is the height of the free surface. For simplicity, we have restricted ourselves to the plane geometry. It should be noted that the problems associated with horizontal differencing in this simplified system are also present in multi-level numerical models.

Designing a finite-difference scheme we have to observe several, often conflicting, criteria which can be summarized as follows:

(i) Simulation of dynamical processes;
(ii) Computational economy;
(iii) Programming considerations (such as storage requirements, indexing, vectorization etc.).

Of course, the final decision is always a compromise between all these requirements. However, the first criterion, obviously, deserves special attention.

As pointed out first by Arakawa, an important decision influencing the performance of finite-difference schemes is the choice of horizontal grid. Several grids used in numerical models are shown in Fig. 1.1. Following Arakawa (e.g. Arakawa and Lamb, 1977) we have denoted them by letters A to E. The A grid is often called "non-staggered" in contrast to the "staggered" grids C and D. The grids B and E, with both velocity components defined at the same point, we shall call "semi-staggered". It should be noted that the only difference between grids B and E is that they are rotated for an angle of 45° with respect to each other. In addition to the rectangular grids A to E, attempts have been made to use hexagonal grids (Sadourny and Morel, 1969).

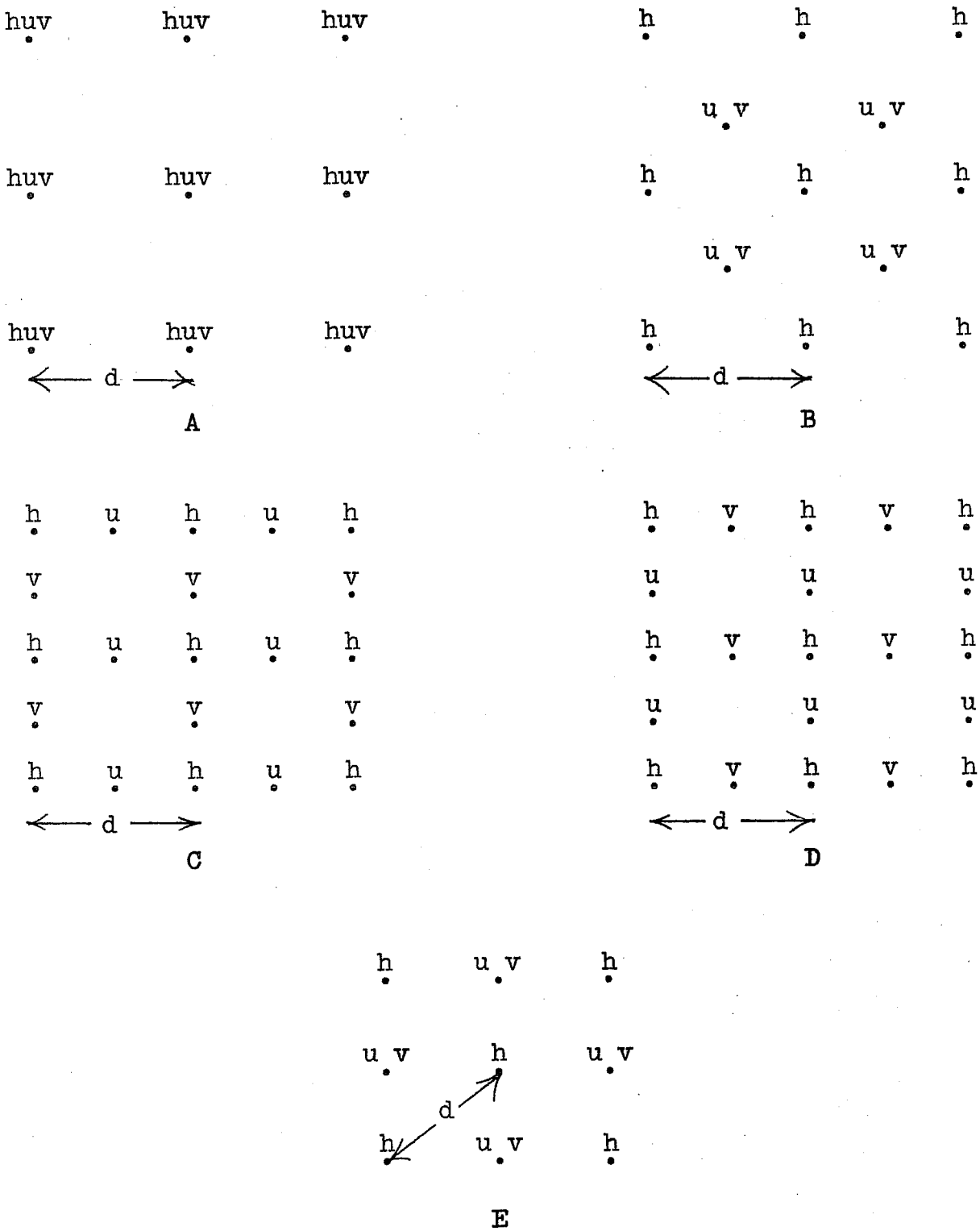

Fig. 1.1. Various arrangements of dependent variables on the rectangular grid.

The problem that we are facing now is how to make a choice among he grids discussed so far and some more that can be designed. The pproach adopted here is to examine the impact of the grid type on the imulation of important physical processes by second-order accurate inite-difference approximations. We shall divide our analysis into two arts. In the first part we shall review the problems present in the inearized equations. Few comments on computational economy and rogramming will be made as well. In the second part we shall discuss ertain aspects of the problems associated with the design of the schemes or non-linear advection terms.

2. LINEARIZED EQUATIONS

2.1 Geostrophic adjustment

Following Winninghoff and Arakawa (e.g. Arakawa and Lamb, 1977), we shall here examine the deterioration of the frequencies of gravity-inertia waves due to second-order accuracy horizontal differencing on various rectangular grids. We shall assume that the distance d between nearest grid points carrying the same variable is the same on all grids. Taking the shallow water at rest with constant Coriolis parameter as the basic state, upon linearization of (1.1), for the grids A - E we obtain

$$\frac{\partial u}{\partial t} = -g\delta_x \bar{h}^x + fv\,, \quad \frac{\partial v}{\partial t} = -g\delta_y \bar{h}^y - fu\,, \qquad \frac{\partial h}{\partial t} = -H(\delta_x \bar{u}^x + \delta_y \bar{v}^y)\,; \tag{2.1$_A$}$$

$$\frac{\partial u}{\partial t} = -g\delta_x \bar{h}^y + fv\,, \quad \frac{\partial v}{\partial t} = -g\delta_y \bar{h}^x - fu\,, \qquad \frac{\partial h}{\partial t} = -H(\delta_x \bar{u}^y + \delta_y \bar{v}^x)\,; \tag{2.1$_B$}$$

$$\frac{\partial u}{\partial t} = -g\delta_x h + f\bar{v}^{xy}\,, \quad \frac{\partial v}{\partial t} = -g\delta_y h - f\bar{u}^{xy}\,, \qquad \frac{\partial h}{\partial t} = -H(\delta_x u + \delta_y v)\,; \tag{2.1$_C$}$$

$$\frac{\partial u}{\partial t} = -g\delta_x \bar{h}^{xy} + f\bar{v}^{xy}\,, \quad \frac{\partial v}{\partial t} = -g\delta_y \bar{h}^{xy} - f\bar{u}^{xy}\,, \qquad \frac{\partial h}{\partial t} = -H(\delta_x \bar{u}^{xy} + \delta_y \bar{v}^{xy})\,; \tag{2.1$_D$}$$

$$\frac{\partial u}{\partial t} = -g\delta_x h + fv\,, \quad \frac{\partial v}{\partial t} = -g\delta_y h - fu\,, \qquad \frac{\partial h}{\partial t} = -H(\delta_x u + \delta_y v)\,. \tag{2.1$_E$}$$

Here, the symbols δ_x and δ_y represent the most straightforward second-order accurate approximations to the horizontal derivatives, and the overbar denotes the two point averaging operator or its repeated application in the direction of coordinate axes indicated by the accompanying superscripts. The mean depth of the fluid is denoted by H.

In order to isolate the horizontal differencing problem, the time derivatives are kept in the differential form. In this way, the

analysis also applies to the time-staggered grids which reduce to the grids A - E in the limit as the time increment tends to zero. The so called Elliasen grid (e.g. Mesinger and Arakawa, 1976) consisting of two time staggered D grids is an example of such a scheme. In this case, in the limit we obtain the E grid.

Substituting into (2.1_A)-(2.1_E) the solution of the form

$$\begin{bmatrix} u \\ v \\ h \end{bmatrix} = \mathrm{Re}\left[\begin{bmatrix} \hat{u} \\ \hat{v} \\ \hat{h} \end{bmatrix} e^{i(kx+\ell y-\nu t)} \right],$$

where $\hat{u}$, $\hat{v}$ and $\hat{h}$ are amplitudes, k and ℓ wave-number components and ν frequency, and introducing the radius of deformation

$$\lambda = \frac{\sqrt{gH}}{f},$$

we obtain the corresponding frequency equations

$$\left(\frac{\nu}{f}\right)^2 = 1 + \left(\frac{\lambda}{d}\right)^2 (\sin^2 kd + \sin^2 \ell d), \qquad (2.2_A)$$

$$\left(\frac{\nu}{f}\right)^2 = 1 + 4\left(\frac{\lambda}{d}\right)^2 \left(\cos^2 \frac{\ell d}{2} \sin^2 \frac{kd}{2} + \cos^2 \frac{kd}{2} \sin^2 \frac{\ell d}{2}\right), \qquad (2.2_B)$$

$$\left(\frac{\nu}{f}\right)^2 = \cos^2 \frac{kd}{2} \cos^2 \frac{\ell d}{2} + 4\left(\frac{\lambda}{d}\right)^2 \left(\sin^2 \frac{kd}{2} + \sin^2 \frac{\ell d}{2}\right), \qquad (2.2_C)$$

$$\left(\frac{\nu}{f}\right)^2 = \cos^2 \frac{kd}{2} \cos^2 \frac{\ell d}{2} + 4\left(\frac{\lambda}{d}\right)^2 \left(\cos^2 \frac{\ell d}{2} \sin^2 kd + \cos^2 \frac{kd}{2} \sin^2 \ell d\right), \qquad (2.2_D)$$

$$\left(\frac{\nu}{f}\right)^2 = 1 + \left(\frac{\lambda}{d}\right)^2 \left(\sin^2 \frac{kd}{\sqrt{2}} + \sin^2 \frac{\ell d}{\sqrt{2}}\right). \qquad (2.2_E)$$

The ratios $|\nu|/f$ calculated in the admissible wave-number ranges from (2.2_A)-(2.2_E) for $\frac{\lambda}{d} = 2$ are shown in Fig 2.1 together with the ratio corresponding to the continuous case (Arakawa and Lamb, 1977). In contrast to the continuous case, for a fixed orientation of the wave number vector, the frequencies reach their maximum values at the points lying on the dashed-dotted lines and decrease as the intensities of the wave-number vectors increase in the shaded areas of the diagrams. Thus, both the intensity and the orientation of the group velocity vector may be substantially altered.

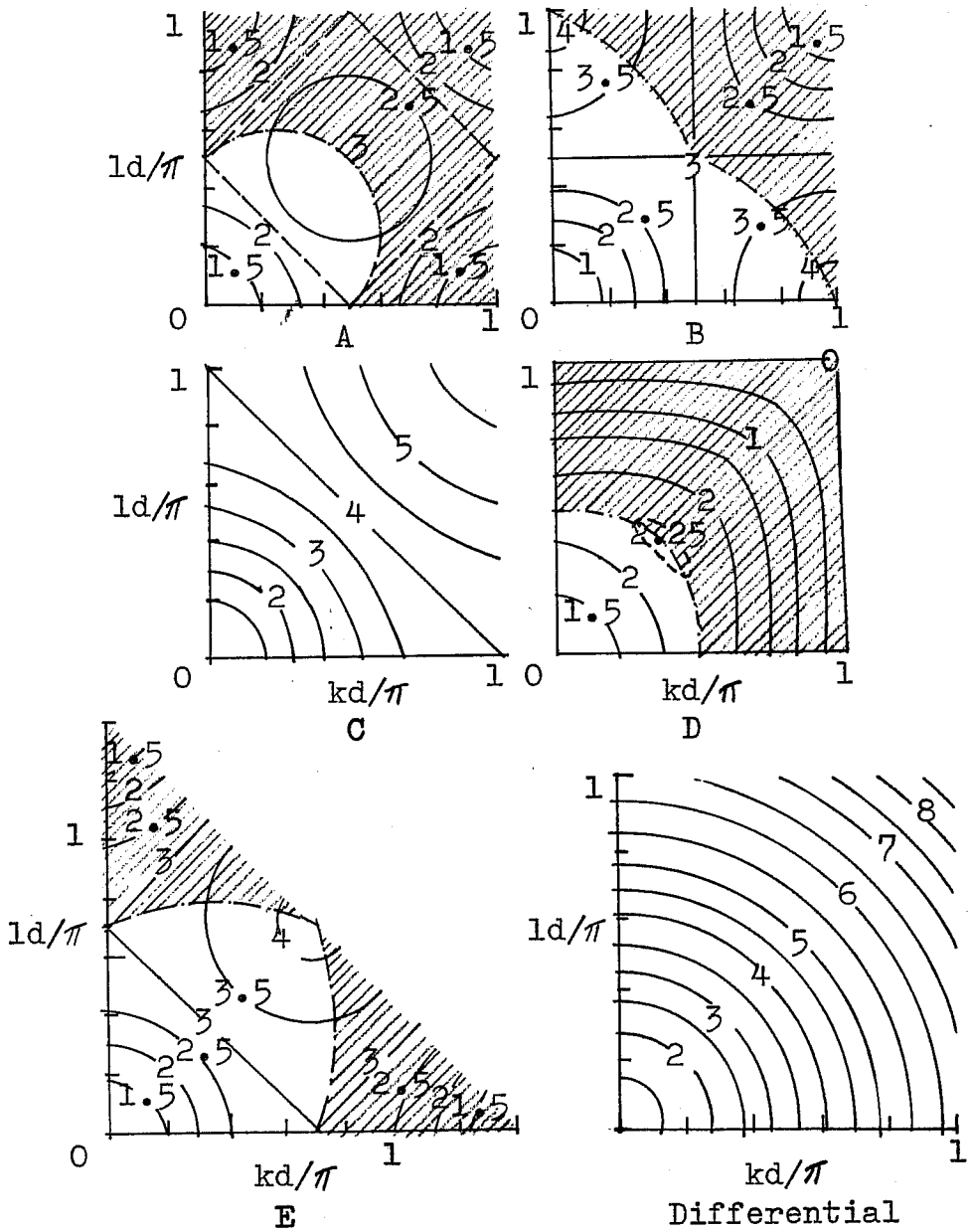

Fig. 2.1. Non-dimensional frequencies $|\nu|/f$ calculated using $\lambda/d=2$ for various grids and the exact non-dimensionalized frequency as functions of non-dimensional wave-number. (After Arakawa and Lamb, 1977)

On the C grid this occurs only at the points $kd = \pi$, $ld = 0$; $kd = 0$, $ld = \pi$ and $kd = \pi$, $ld = \pi$ where the group velocity vanishes. However, a closer inspection of the frequency equation (2.2_C) reveals that in the case of higher internal modes, when λ/d is small, the frequency will be seriously distorted in the overwhelming portion of the admissible wave-number range.

The B and E grid diagrams can be obtained from each other by rotation of the k, l axes. This is not unexpected since an analogous coordinate transformation in the physical space shows that the systems (2.1_B) and (2.1_E) are equivalent (Mesinger and Arakawa, 1976; Janjić, 1979). As compared to the grids A and D, the shaded areas for these two grids are much smaller. Also, since there is no averaging of the Coriolis force terms, there is no distortion of the frequency diagram for small λ/d ratios. Namely, if λ/d is small, the Coriolis terms are dominating and the relative frequency error is even reduced.

From these considerations we conclude that for the external and lower internal modes the C grid is best. However, the grids B and E are better than the grid C for higher internal modes. As we shall see later on, using a special technique, the difficulties encountered on the grids B and E for large λ/d ratios can be to a large extent reduced.

2.2 Rossby wave phase speeds

Following Mesinger (1979), we shall now examine the effect of the grid choice on the Rossby wave phase speeds. Namely, let us consider the linearized shallow water equations in the β plane

$$\frac{\partial u}{\partial t} + U\frac{\partial u}{\partial x} - (f_0 + \beta y)v + g\frac{\partial h}{\partial x} = 0 ,$$
$$\frac{\partial v}{\partial t} + U\frac{\partial v}{\partial x} + (f_0 + \beta y)u + g\frac{\partial h}{\partial y} = 0 . \qquad (2.3)$$

Here, U is the basic current. For each of the five lattices A - E we shall again use the simplest centered second-order approximations for the space derivatives and the Coriolis terms. However, this time we are interested in the vorticity equation analogues that correspond to each of the five finite-difference systems. In order to form these analogues

we want to follow the procedure of the differential case. It is, however, not obvious in all of the five difference cases which operators are appropriate to an analogous procedure. Namely, with the lattice A differencing over a single grid distance and over two grid distances can be considered. The former would lead to a more accurate definition of vorticity; however, this more accurate vorticity would be subject to a false generation by the pressure gradient force. The experience gained with numerical models shows that, in general, avoiding the generation of a physically important quantity for false reasons should be given priority over the desire for a formal increase in accuracy. Therefore, as an analogue of the vorticity equation we shall consider a finite -difference scheme achieving highest accuracy for the given lattice on the condition that it contains no terms depending on geopotential gh.

With this requirement we obtain, as the vorticity equation analogues

$$\frac{\partial}{\partial t}\left(\overline{\delta_x v}^{x} - \overline{\delta_y u}^{y}\right) + U\overline{\delta_x\left(\overline{\delta_x v}^{x} - \overline{\delta_y u}^{y}\right)}^{x} + (f_0 + \beta y)\left(\overline{\delta_x u}^{x} + \overline{\delta_y v}^{y}\right) + \beta\,\overline{v}^{yy} = 0\,, \tag{2.4$_A$}$$

$$\frac{\partial}{\partial t}\left(\overline{\delta_x v}^{y} - \overline{\delta_y u}^{x}\right) + U\,\overline{\delta_x\left(\overline{\delta_x v}^{y} - \overline{\delta_y u}^{x}\right)}^{x} + (f_0 + \beta y)\left(\overline{\delta_x u}^{y} + \overline{\delta_y v}^{x}\right) + \beta\,\overline{v}^{xy} = 0\,, \tag{2.4$_B$}$$

$$\frac{\partial}{\partial t}\left(\delta_x v - \delta_y u\right) + U\,\overline{\delta_x(\delta_x v - \delta_y u)}^{x} + (f_0 + \beta y)\,\overline{(\delta_x u + \delta_y v)}^{xy} + \beta\,\overline{v}^{xyy} = 0\,, \tag{2.4$_{C,D}$}$$

$$\frac{\partial}{\partial t}\left(\delta_x v - \delta_y u\right) + U\,\overline{\delta_x(\delta_x v - \delta_y u)}^{y} + (f_0 + \beta y)\left(\delta_x u + \delta_y v\right) + \beta\,\overline{v}^{y} = 0\,. \tag{2.4$_E$}$$

As indicated by the subscripts of numbers identifying these equations, the vorticity analogues obtained with lattices C and D are of the same form.

Obviously, the analogues (2.4_A)-(2.4_E) imply that for considered lattices one should define the vorticity by

$$\zeta \equiv \overline{\delta_x v}^{x} - \overline{\delta_y u}^{y} , \qquad (2.5_A)$$

$$\zeta \equiv \overline{\delta_x v}^{y} - \overline{\delta_y u}^{x} , \qquad (2.5_B)$$

$$\zeta \equiv \delta_x v - \delta_y u . \qquad (2.5_{C,D,E})$$

Definitions of divergence consistent with (2.5_A)-$(2.5_{C,D,E})$ are seen to be

$$\nabla_+ \cdot \mathbf{v} \equiv \overline{\delta_x u}^{x} + \overline{\delta_x v}^{y} , \qquad (2.6_A)$$

$$\nabla_+ \cdot \mathbf{v} \equiv \overline{\delta_x u}^{y} + \overline{\delta_y v}^{x} , \qquad (2.6_B)$$

$$\nabla_+ \cdot \mathbf{v} \equiv \delta_x u + \delta_y v . \qquad (2.6_{C,D,E})$$

The vorticity and divergence definitions obtained for the A grid are of the poorest accuracy, with no obvious compensation in some other property of the system. Transformation of coordinates shows that the vorticity and divergence definitions for the B and E lattice are, in fact, equivalent; therefore they are of the same accuracy. However, in contrast to the gravity-inertia waves, due to the β effect, the Rossby wave propagation is not independent on the rotation of the grid, and, therefore, we should expect different behaviour on the two lattices. The vorticity and divergence definitions on the C and D lattice are of the highest accuracy. However, on these lattices the vorticity and divergence are not defined at the same grid points, and some loss in accuracy results in the divergence term of $(2.4_{C,D})$, owing to the four-point averaging of the velocity divergence.

For a further analysis of the effects of truncation on the phase speeds of the Rossby waves, we require

$$\nabla \cdot \mathbf{v} = 0 , \qquad (2.7)$$

and accordingly

$$\nabla_+ \cdot \mathbf{v} = 0 . \qquad (2.8)$$

a. Rossby wave phase speeds

We shall consider first the effect of the β term only, that is the case

$$U = 0 . \tag{2.9}$$

In the differential case, substituting

$$\begin{bmatrix} u \\ v \end{bmatrix} = \mathrm{Re}\left[\begin{bmatrix} \hat{u} \\ \hat{v} \end{bmatrix} e^{ik(x-ct)}\right]$$

into the vorticity equation, we obtain, in view of (2.7) and (2.9)

$$c = -\frac{\beta}{k^2} \tag{2.10}$$

The analogous procedure, performed for difference cases gives the phase speeds

$$c^* = -\frac{\beta}{k^2}\,\frac{kd}{\sin kd} \tag{2.11_A}$$

$$c^* = -\frac{\beta}{k^2}\,\frac{kd/2}{\tan kd/2} \tag{$2.11_{B,C,D}$}$$

$$c^* = -\frac{\beta}{k^2}\,\frac{kd/\sqrt{2}}{\sin kd/\sqrt{2}} \quad . \tag{2.11_E}$$

The values of the phase speeds (2.10) and (2.11_A)-(2.11_E) in non-dimensional units, $c/\beta d^2$, as the functions of non-dimensional wave number kd/π, are shown in Fig. 2.2. Since the true phase speed c is negative, for longer waves, the lattices A and E are seen to have a decelerating effect, and the lattices B, C and D an accelerating effect. The relative phase speed errors of the lattices B, C, D and E are found to be, in this wave-number range, about the same and approximately twice smaller than those of the A lattice. Note that, with the lattices A and E, when the wave length approaches the two-grid-intervals, the vorticity defined by (2.5_A) and ($2.5_{C,D,E}$) tends to zero. Thus, the unbounded increase in absolute values of phase speeds, seen in Fig. 2.2, is associated with the vanishing values of the finite-difference vorticity analogues.

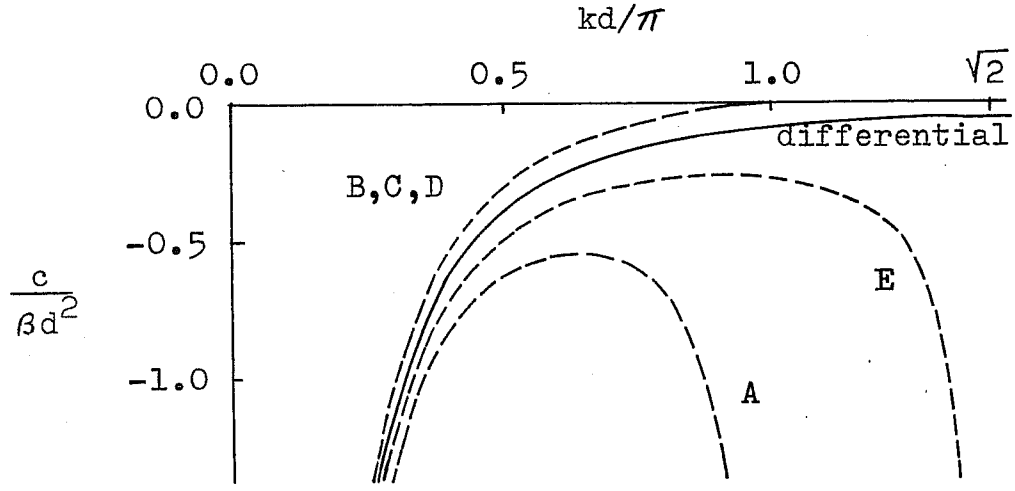

Fig. 2.2. Phase speeds (2.10) and (2.11_A)-(2.11_E) in non-dimensional units $c/\beta d^2$ as functions of non-dimensional wave-number kd/π. (After Mesinger, 1979)

b. **Effect of the advection terms**

With advection terms included, that is

$$U \neq 0 ,$$

substitution of wave solutions into the exact and finite-difference vorticity equations gives the phase speeds

$$c = U - \frac{\beta}{k^2} \qquad (2.12)$$

and

$$c^* = U \frac{\sin kd}{kd} - \frac{\beta}{k^2} \frac{kd}{\sin kd} , \qquad (2.13_A)$$

$$c^* = U \frac{\sin kd}{kd} - \frac{\beta}{k^2} \frac{kd/2}{\tan kd/2} , \qquad (2.13_{B,C,D})$$

$$c^* = U \frac{\sin kd/\sqrt{2}}{kd/\sqrt{2}} - \frac{\beta}{k^2} \frac{kd/\sqrt{2}}{\sin kd/\sqrt{2}} , \qquad (2.13_E)$$

respectively.

The advection terms in (2.13_A)-(2.13_E) illustrate a familiar decelerating effect of the centred second-order space differencing. Furthermore, a notable difference is seen between the "parallel" orientation of grids A, B, C and D, and the "diagonal" orientation of grid E. The diagonal orientation for zonal advection is seen to result in a smaller phase error.

For the wave lengths which are not close to two grid intervals, in the expressions (2.13_A) through (2.13_E), the error of the advection term will dominate over that of the β term when the non-dimensional ratio $U/\beta d^2$ is much greater than 1. This ratio is indeed much greater than 1 for typical zonal speeds and grid sizes; for example, the values $U \sim 10$ m s^{-1} and $d \sim 250$ km give the ratio $U/\beta d^2 \sim 10$.

One should, however, not overestimate the importance of numerical details of the phase speed error of advection terms in (2.13_A)-(2.13_E). Namely, various grids may have a different effect on the vorticity advection when the Arakawa-type formulation is used for the advection

terms - an approach that seems to be gaining in popularity.

2. Summary

Summarizing, we may say that the non-staggered grid A exhibit a distinct disadvantage in that the second-order vorticity analogue of the highest local accuracy is associated with a spurious vorticity production by the pressure gradient force. The next most accurate second-order analogue, not suffering from this drawback, is of a poor accuracy compared to such analogues on the staggered and semi-staggered grids B, C, D and E.

The analysis of Rossby wave phase speeds, resulting from the considered vorticity equation analogues, again shows a disadvantage of the non-staggered grid. The phase speed error of the β term on the non-staggered grid is greater than on staggered and semi-staggered grids and is of the same sign as that of the advection terms - with difference formulations such as usually used in atmospheric models.

As for the four staggered and semi-staggered grids considered here, a simple general statement on the grid preference, as far as the vorticity equation analogues are concerned, cannot be made. The staggered grids C and D allow most accurate second-order vorticity analogues; however, in the divergence and the β term they require more averaging than the semi-staggered grids B and E. The sign and magnitude of the corresponding Rossby wave phase speeds depend on the flow and solution parameters - advection speed and the zonal and meridional wave numbers. Considering the effect of the β term only, the relative phase speed error on these four grids is for longer waves about the same, approximately twice smaller than that on the non-staggered grid.

2.3 Barotropic instability

Another dynamical process governed by linearized equations which has been investigated to increase understanding of the properties of various horizontal grids is that of barotropic instability (Ničković, 1979). The particular mechanism analyzed was that described by shallow water equations for non-divergent flow, with a constant Coriolis

parameter, and linearized about a zonal mean wind $U(y)$. Considering a zonal profile with a constant shear dU/dy within a bounded domain $-\ell < y < \ell$, and no shear north and south of that domain (Fig. 2.3) Haurwitz (1943) obtains the phase speed of simple wave solutions

$$c = \bar{U} + U_* \left[1 - \frac{2}{\omega} + \frac{1}{\omega^2}(1 - e^{-2\omega})\right]^{1/2} . \qquad (2.14)$$

Here

$$\omega \equiv 2k\ell , \quad \bar{U} \equiv \tfrac{1}{2}(U_1 + U_3) , \quad U_* \equiv \tfrac{1}{2}(U_3 - U_1) .$$

Examination of (2.14) shows the existence of unstable waves. Waves longer than about one-fifth of the width of the middle layer are unstable due to meridional wind shear. Thus, the narrower the middle layer, the wider will be the instability wavenumber zone.

Ničković has reproduced this stability analysis for three types of horizontal grids, A, C and E. He has left the time derivatives in their continuous form, and he has used the simplest second-order approximations to the pressure gradient force. For advection terms he has used

for grid A - Grammeltvedt (1969) energy conserving scheme (scheme E in his notation)
for grid C - Sadourny (1975) energy conserving scheme
for grid E - Janjić (1977) energy and enstrophy conserving scheme.

It is interesting to note that Grammeltvedt and Sadourny schemes reduce to the simplest space-centred schemes after linearization. There is also an equivalence between linearized forms of energy and enstrophy schemes proposed by Sadourny (1975).

The resulting growth-rate functions computed assuming $\ell = d$ for grids A and C, and $\ell = d/\sqrt{2}$ for grid E are presented in the following figures. For grid E, very little difference between the differential and the finite-difference growth rate was obtained (Fig. 2.4). A slightly greater, but still quite small, was the difference obtained using the grid C (Fig. 2.5, left half). For grid A, however, an additional region of false instability was obtained for high wave-numbers (same figure, right half).

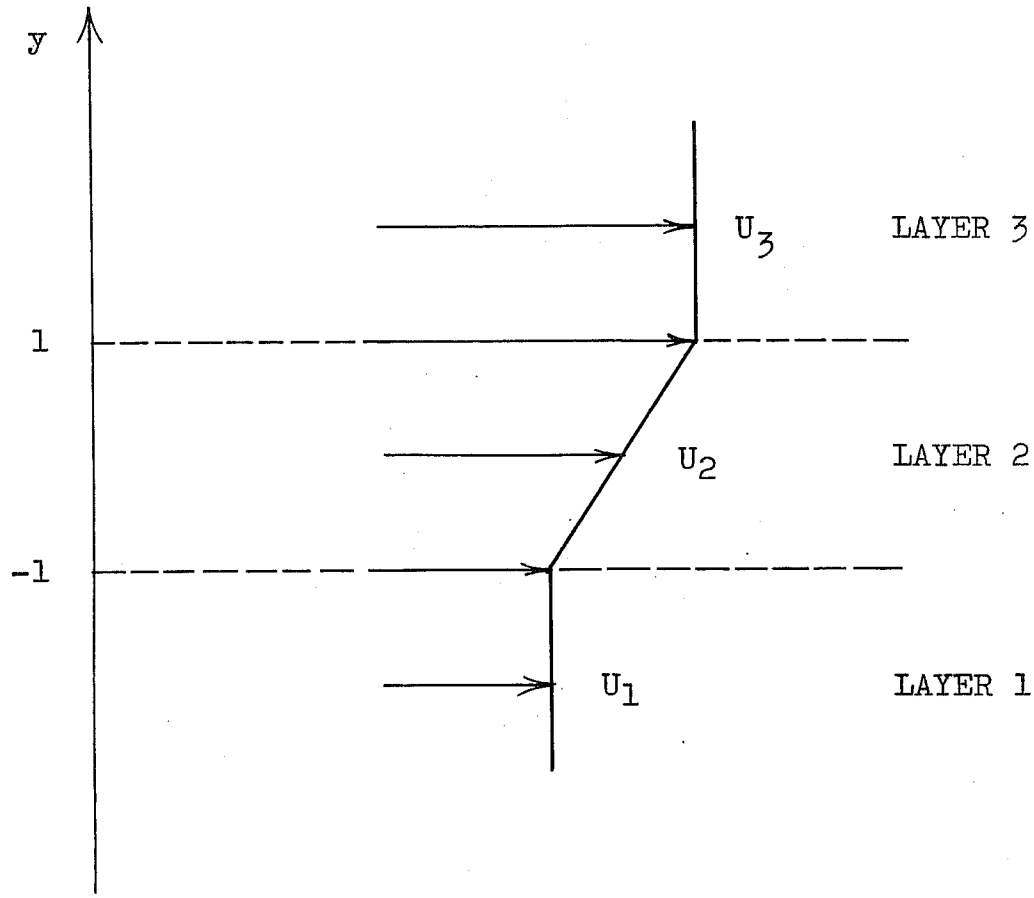

Fig. 2.3. Horizontal profile of the mean zonal wind. (After Ničković, 1979)

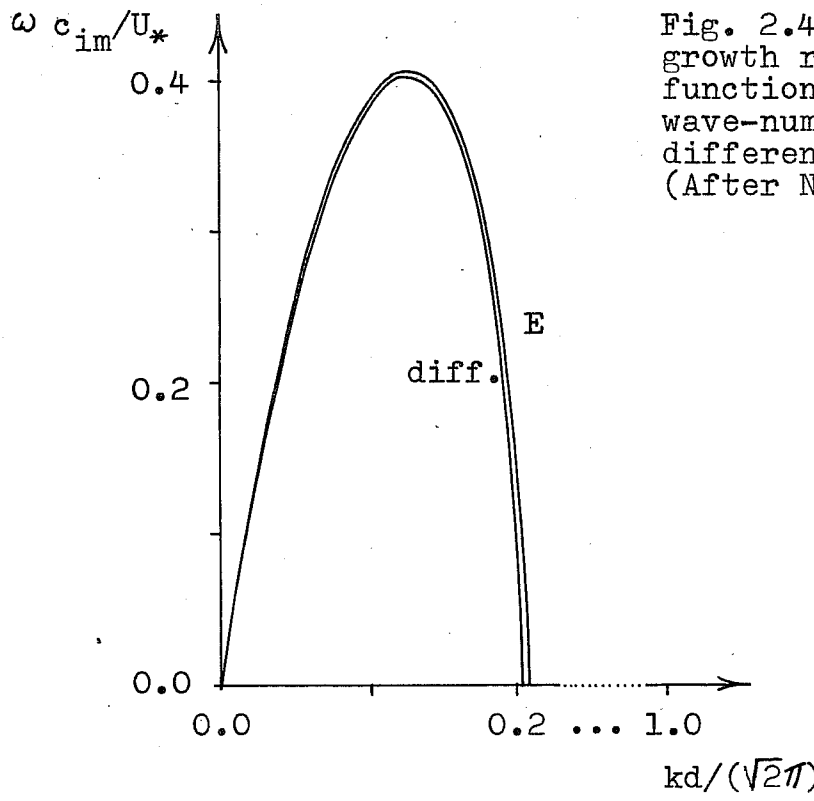

Fig. 2.4. Non-dimensional growth rates $\omega c_{im}/U_*$ as functions of non-dinensional wave-number $kd/(\sqrt{2}\pi)$ for differential case and grid E. (After Ničković, 1979)

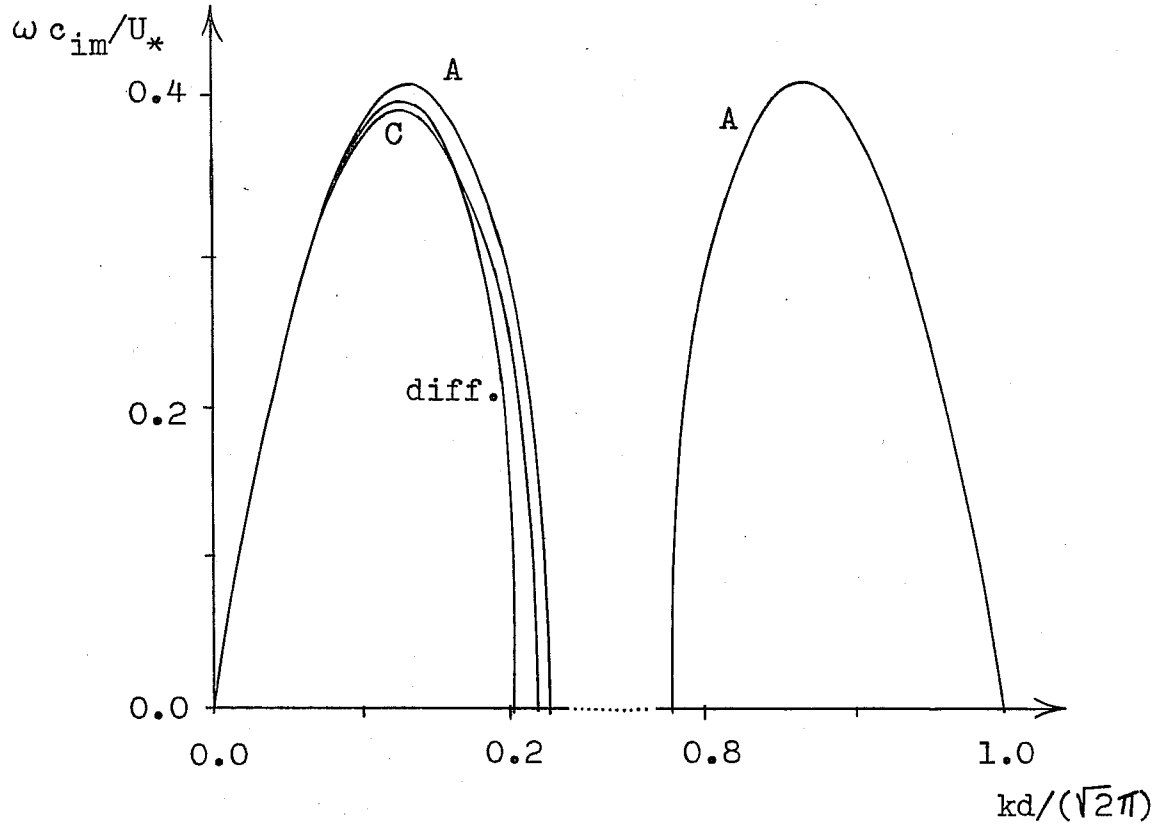

Fig. 2.5. Non-dimensional growth rates $\omega c_{im}/U_*$ as functions of non-dimensional wave number $kd/(\sqrt{2}\pi)$ for differential case and grids A and C. (After Ničković, 1979)

Effects of this instability in actual numerical integrations using the A grid may have been obscured due to usual damping applied with the non-staggered grid. In that case instability would be expected to increase the requirements for the intensity of damping, thereby also increasing the undesirable effects of the damping on longer meteorologically significant waves of the model. In addition, an increased intensity of damping of short waves distorts the effects of short wave forcing mechanisms that may and frequently are present in atmospheric models. Thus, the appearance of false short-wave instability can certainly be considered as another disturbing property of the non-staggered horizontal grid.

2.4 Technique preventing grid separation on semi-staggered grids

As we have seen in Section 2.1, an unpleasant feature of the semi-staggered grids B and E is that the frequency of the gravity-inertia waves is decreasing as we approach the shortest resolvable scales. In this section we shall look at this problem in some detail and discuss a possible remedy.

For convenience, we choose the E grid for our analysis. As shown in Fig. 2.6, this type of grid can be decomposed into two C subgrids carrying circled and squared variables respectively. However, direct inspection of the system

$$\frac{\partial u}{\partial t} = -g\,\delta_x h \quad , \quad \frac{\partial v}{\partial t} = -g\,\delta_y h \quad , \quad \frac{\partial h}{\partial t} = -H(\delta_x u + \delta_y v)$$

governing the propagation of gravity waves, reveals that a disturbance on the subgrid with squared variables cannot be transferred to the subgrid with circled variables and vice versa. Namely, the grid point at which the tendency is calculated and the grid points carrying the variables needed to calculate it, belong to the same C subgrid. Thus, the gravity waves defined on the two subgrids will propagate independently. For example, two decoupled large-scale solutions, when viewed together, will produce a slowly changing pattern with predominant small scale features. In particular, two different stationary solutions for h will be interpretted by the E grid as a zero-frequency two-grid -interval wave.

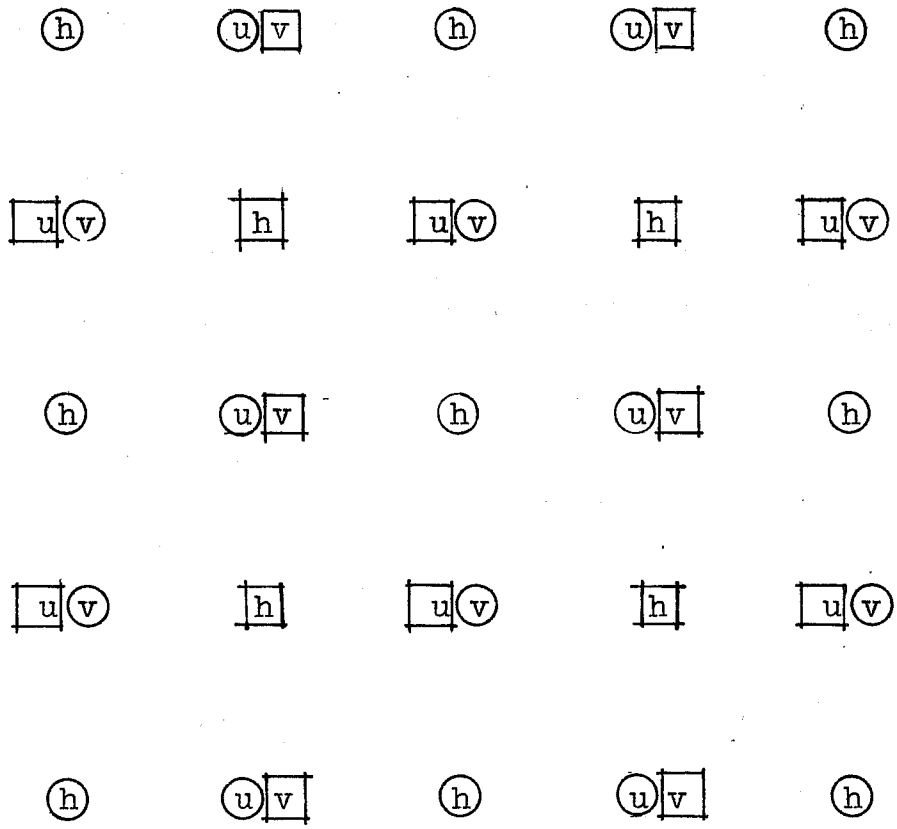

Fig. 2.6. Grid E decomposed into two C subgrids carrying circled and squared variables respectively. (After Janjić, 1979)

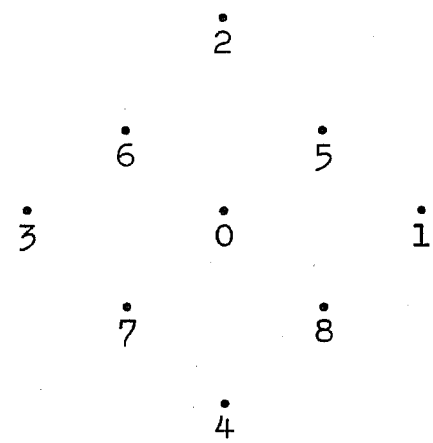

Fig. 2.7. Stencil used to define two different approximations to Laplacian on the E grid.

In the case of complete shallow water equations, due to the presence of Coriolis and advection terms, there is a possibility of interaction of the decoupled gravity wave solutions. However, this interaction is slow compared to that due to gravity wave propagation, and being incomplete it does not provide physically justified communication between adjacent grid points belonging to different subgrids.

Damping or chopping of the small-scale part of the spectrum (Gerrity and McPherson, 1970; Shapiro, 1970; Haltiner, 1971) has been traditionally used in numerical models to remove the small scale noise resulting from the grid separation. However, an alternative approach was proposed by Arakawa (1972) and Mesinger (1973). Their idea was that instead of attacking the consequences of inadequacies in a simulation of a physical process, it was generally advantageous to look for a method that would achieve a physically correct simulation of the process, and thus eliminate the cause of the difficulty (Mesinger and Arakawa, 1976).

In contrast to Arakawa's (1972) "time-alternating-space-uncentred" (TASU) scheme for the B grid, the technique proposed by Mesinger (1973) strictly preserves second order accuracy of the spatial differencing. This technique has been applied to a number of time differencing schemes (Mesinger, 1973, 1974; Mesinger and Arakawa, 1976; Janjić, 1974, 1979). Following the papers by Janjić (1979) and Vasiljević (1982) we shall here demonstrate its application and examine the properties of the resulting scheme using the example of the forward-backward time integration procedure.

a. Derivation of the scheme

To indicate the procedure which can be used in the case of complete shallow water equations, we start from the system

$$u^{\tau+1} = u^{\tau} - \Delta t g \delta_x h^{\tau+1} + \Delta t C_x + \Delta t A_u \ ,$$

$$v^{\tau+1} = v^{\tau} - \Delta t g \delta_y h^{\tau+1} + \Delta t C_y + \Delta t A_v \ , \qquad (2.15)$$

$$h^{\tau+1} = h^{\tau} - \Delta t \left[\nabla_{\cdot} \cdot (h_* v) \right]_*^{\tau} \ .$$

Here A_u and A_v, and C_x and C_y are the x and y components of the advection vector A_v and the Coriolis force $\mathbb{C}$, respectively. There is a number of space and time differencing schemes which can be used for these terms in combination with the forward-backward scheme. However, since they are irrelevant for the present considerations, there is no need to restrict the generality of the analysis by any particular choice. For this reason, the schemes for the advection and Coriolis terms are not indicated here. The symbol h_* denotes the value of h at a velocity point whatever its definition may be.

We define the expression $[\nabla_+ \cdot (h_* v)]_*^\tau$ by

$$[\nabla_+ \cdot (h_* v)]_*^\tau \equiv H(\nabla_+ \cdot v)_*^\tau + \nabla_+ \cdot [(h_* - H) v]^\tau \tag{2.16}$$

To define $(\nabla_+ \cdot v)_*^\tau$ we use the finite-difference divergence equation of the form

$$(\nabla_+ \cdot v)_*^\tau = (\nabla_+ \cdot v)^{\tau-1} - \Delta t g [(1-w)\nabla_+^2 + w \nabla_x^2] h^\tau + \Delta t \nabla_+ \cdot \mathbb{C} + \Delta t \nabla_+ \cdot A_v \quad . \tag{2.17}$$

Here, at point 0 in Fig. 2.7, the finite difference Laplacians appearing in (2.17) are defined by

$$\nabla_+^2 Z \equiv (\delta_{xx} + \delta_{yy}) Z \equiv \frac{Z_1 + Z_2 + Z_3 + Z_4 - 4Z_0}{2d^2} \quad ,$$

$$\nabla_x^2 Z \equiv \frac{Z_5 + Z_6 + Z_7 + Z_8 - 4Z_0}{d^2} \quad .$$

and the symbol w denotes a weighting factor.

It can be easily verified that when $w > 0$ the approximation (2.17) allows the gravity waves to propagate through the entire E grid. Namely, the approximation to the Laplacian is responsible for excitation of disturbances in the divergence field, which in turn disturb the height field. Since with the present definition of the Laplacian in (2.17) we calculate the divergence taking into account the changes due to the disturbances in the height field at both elementary C subgrids, it is guaranteed that a disturbance excited at any of the grid points will be transferred by the gravity waves throughout the E grid. It should be noted, however, that the definition (2.17) implies that there is no

separation at the time level $\tau - 1$.

From the first two of Eqs. (2.15) we obtain

$$(\nabla_+ \cdot \mathbf{v})^\tau = (\nabla_+ \cdot \mathbf{v})^{\tau-1} - \Delta t g \nabla_+^2 h^\tau + \Delta t \nabla_+ \cdot \mathbf{C} + \Delta t \nabla_+ \cdot \mathbf{A}_\mathbf{v} . \tag{2.18}$$

On the other hand, rearranging (2.17) we may write

$$(\nabla_+ \cdot \mathbf{v})^\tau_* = (\nabla_+ \cdot \mathbf{v})^{\tau-1} - \Delta t g \nabla_+^2 h^\tau + \Delta t \nabla_+ \cdot \mathbf{C} + \Delta t \nabla_+ \cdot \mathbf{A}_\mathbf{v} - \Delta t w g [\nabla_x^2 - \nabla_+^2] h^\tau . \tag{2.19}$$

Combining (2.18) and (2.19) we obtain

$$(\nabla_+ \cdot \mathbf{v})^\tau_* = (\nabla_+ \cdot \mathbf{v})^\tau - \Delta t w g [\nabla_x^2 - \nabla_+^2] h^\tau \tag{2.20}$$

Substituting (2.20) into (2.16) we may write

$$[\nabla_+ \cdot (h_* \mathbf{v})]^\tau_* = H(\nabla_+ \cdot \mathbf{v})^\tau + \nabla_+ \cdot [(h_* - H)\mathbf{v}]^\tau - \Delta t w g H [\nabla_x^2 - \nabla_+^2] h^\tau \tag{2.21}$$

and finally

$$h^{\tau+1} = h^\tau - \Delta t \nabla_+ \cdot (h_* \mathbf{v})^\tau + (\Delta t)^2 w g H [\nabla_x^2 - \nabla_+^2] h^\tau . \tag{2.22}$$

The only change resulting from the modification is the presence of the last term on the right hand side of (2.22). This term takes on a non-zero value only when finite difference Laplacian is not invariant with respect to rotation for an angle of 45°.

Having derived the modified scheme, let us now turn our attention to its properties.

b. **Stability and phase speed of gravity waves**

For simplicity we shall first consider the pure gravity wave part of the shallow water equations, i.e.,

$$u^{\tau+1} = u^{\tau} - \Delta t\, g\, \delta_x h^{\tau+1}$$

$$v^{\tau+1} = v^{\tau} - \Delta t\, g\, \delta_y h^{\tau+1} \tag{2.23}$$

$$h^{\tau+1} = h^{\tau} - \Delta t\, H\, \nabla_+ \cdot v^{\tau} + (\Delta t)^2 w g H [\nabla_x^2 - \nabla_+^2] h^{\tau} .$$

Defining

$$\lambda \equiv |\lambda| e^{-i\nu\Delta t};\quad X \equiv kd/\sqrt{2};\quad Y \equiv ld/\sqrt{2};\quad \mu \equiv \Delta t/d ,$$

and substituting into the system (2.23) a solution of the form

$$\begin{bmatrix} u^{\tau} \\ v^{\tau} \\ h^{\tau} \end{bmatrix} = \mathrm{Re}\left[\begin{bmatrix} \hat{u} \\ \hat{v} \\ \hat{h} \end{bmatrix} \lambda^{\tau} e^{i(kx+ly)} \right] \tag{2.24}$$

we obtain

$$(\lambda-1)\hat{u} + i\lambda\sqrt{2}\mu g \sin X\, \hat{h} = 0 ,$$

$$(\lambda-1)\hat{v} + i\lambda\sqrt{2}\mu g \sin Y\, \hat{h} = 0 , \tag{2.25}$$

$$i\sqrt{2}\mu H \sin X\, \hat{u} + i\sqrt{2}\mu H \sin Y\, \hat{v} + [\lambda - 1 + 2 w g H \mu^2 (\cos X - \cos Y)^2]\hat{h} = 0 .$$

The three solutions for λ, obtained from the requirement that the determinant of the system (2.25) vanish, are

$$\lambda = 1$$

and

$$\lambda = 1 - (A + wB) \pm \sqrt{(A+wB)^2 - 2A} . \tag{2.26}$$

Here,

$$A \equiv gH/\mu^2(\sin^2 X + \sin^2 Y), \quad B \equiv gH/\mu^2(\cos X - \cos Y).$$

Inspecting the system (2.25) we find that the neutral and stationary solutions with non-zero wave-numbers are allowed in the velocity field, but not in the height field. Namely, if $\lambda = 1$, $\sin^2 X + \sin^2 Y \neq 0$, the amplitude $\hat{h}$ cannot take on non-zero values. Similarly, if $\lambda = 1$, $\sin^2 X + \sin^2 Y = 0$ and $(\cos X - \cos Y)^2 \neq 0$, i.e., the two-grid-interval wave is considered, $\hat{h}$ must again be zero. This is not the case when the conventional forward-backward scheme is used. Then the $(\cos X - \cos Y)^2$ term is absent and false neutral and stationary solution with arbitrary amplitude may exist.

The analysis of the amplification factor $|\lambda|$ corresponding to the non-stationary solutions (2.26) shows that, provided w does not exceed .25, the modification has no effect on the stability of the scheme (e.g. Janjić, 1979).

Figure 2.8 shows the maximum of the two amplification factors calculated from (2.26) with $w = .25$ and $\sqrt{gH}/\mu = .71$. Since the roots (2.26) are symmetric with respect to the lines $|X| = |Y|$ and X and Y axes, to avoid repetition, only the triangular domain between the positive X axis and the line $X = Y$ is shown. Along the line $X = Y$ the term B in (2.26) vanishes and the scheme is neutral. However, along the X axis the damping effect of the modification is most pronounced.

From the definition of λ and (2.26) we find that when $(A + wB)^2 - 2A < 0$, the relative phase speed is given by

$$\frac{c}{\sqrt{gH}} = \frac{1}{\mu\sqrt{2gH(X^2+Y^2)}} \operatorname{atan}\left\{\frac{\sqrt{2A - (A+wB)^2}}{1 - (A+wB)}\right\}.$$

If $(A + wB)^2 - 2A \geq 0$, λ is real and the relative phase speed is zero.

The relative phase speed calculated with $w = .25$ and $\sqrt{gH}/\mu = .71$ is shown in Fig. 2.9. Again only one part of the admissible wave number domain is shown. In the shaded area in Fig. 2.9 the relative phase speed is zero. However, in this area the gravity waves are strongly damped.

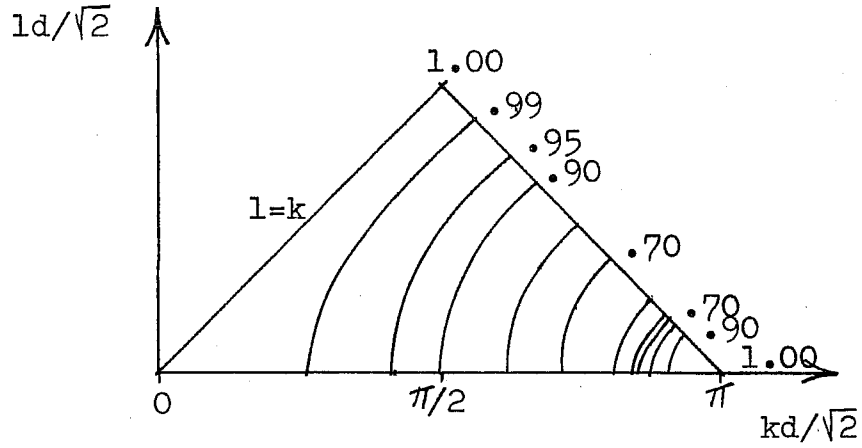

Fig. 2.8. Maximum amplification factor of gravity waves in the case of modified forward-backward scheme. (After Janjić, 1979)

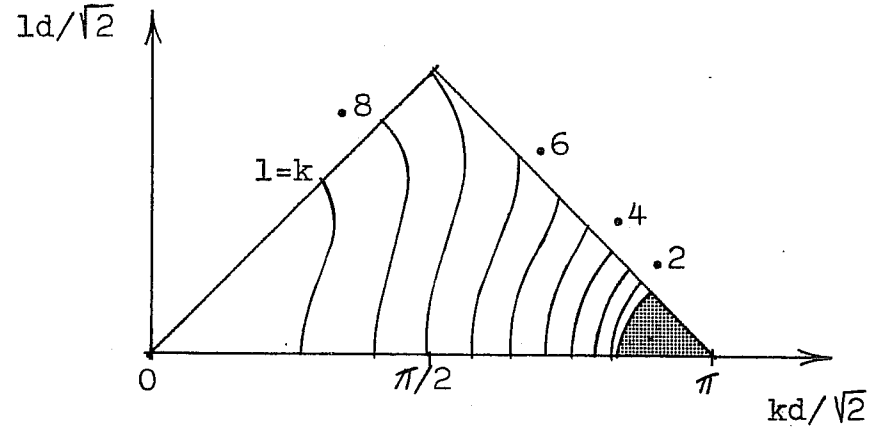

Fig. 2.9. Relative phase speed of gravity waves in the case of modified forward-backward scheme. (After Janjić, 1979)

c. Geostrophic mode

An interesting problem which has not been discussed so far is the effect of the modification on the geostrophic part of the solution. Introducing the Coriolis terms into the system (2.23) we may write

$$u^{\tau+1} = u^{\tau} - \Delta t\, g\, \delta_x h^{\tau+1} + \Delta t\, f\, \tfrac{1}{2}(v^{\tau} + v^{\tau+1}),$$

$$v^{\tau+1} = v^{\tau} - \Delta t\, g\, \delta_y h^{\tau+1} - \Delta t\, f\, \tfrac{1}{2}(u^{\tau} + u^{\tau+1}), \qquad (2.27)$$

$$h^{\tau+1} = h^{\tau} - \Delta t\, H\, \nabla_+ \cdot \mathbf{v}^{\tau} + (\Delta t)^2 w g H [\nabla_x^2 - \nabla_+^2] h^{\tau}.$$

Here, the trapezoidal time-stepping scheme has been chosen for the Coriolis terms (Janjić and Wiin-Nielsen, 1977; Janjić, 1979). Substituting a solution of the form (2.24) into (2.27), and requiring that the determinant of the system obtained in this way be equal to zero, we arrive to the equation

$$[(\lambda-1)^2 + F(\lambda+1)^2](\lambda - 1 + 2wB) + (\lambda-1)\lambda 2A = 0. \qquad (2.28)$$

Here,

$$F \equiv \tfrac{1}{4}(f\Delta t)^2$$

Since the roots of (2.28) are symmetric with respect to the line $|X| = |Y|$ and to the X and Y axes, we shall again restrict ourselves to the triangular domain between the positive X axis and the lines $Y = X$ and $Y = \pi - X$. The values of constants appearing in (2.27) which will be used in our analysis are: $f = .0001\ s^{-1}$, $\Delta t = 450$ s, $\sqrt{gH}\mu = .71$ and $w = .25$.

In the continuous case, the linearized shallow water equations with constant Coriolis parameter allow three solutions. Two of these are the gravity-inertia waves, and the third one is stationary, geostrophic mode. Analogously, dealing with the finite-difference equations, we shall consider the stationary solution as being the geostrophic one, no matter whether its amplitude is damped or amplified. Having in mind the definition of λ, we find that the solution will be

stationary provided λ is real and positive, i.e.,

$$\lambda = |\lambda| \ .$$

Note that this implies that $\nu=0$.

The analysis of the equation (2.28) shows that for the shortest waves, including the two-grid interval wave, λ is real and negative, and therefore, the geostrophic solution is non-existent. However, there is a region within the large wave-number range in which all three roots are real and positive, and hence, in this region the geostrophic solution cannot be identified applying our criterion. The values of the amplification factor of the geostrophic mode are shown in Fig. 2.10. In the lightly shaded area in the figure all three roots are real and positive. The isolines shown in this area correspond to the maximum of the three roots. In the heavily shaded area the geostrophic mode is non-existent.

Let us now examine the effect of the linear diffusion as a possible alternative remedy for the low frequency short-wave noise resulting from the grid separation. For this purpose we shall use the second and fourth degree linear diffusion of velocity. Namely, in the case of the second degree diffusion we shall introduce into the equations of motion the terms $K\nabla_x^2 u^\tau$ and $K\nabla_x^2 v^\tau$. On the other hand, we shall assume that the fourth order terms have the form $K'\nabla_x^2(\nabla_x^2 u^\tau)$ and $K'\nabla_x^2(\nabla_x^2 v^\tau)$. Of course, we shall switch off the modification by setting $w=0$ in the continuity equation.

Instead of (2.28), this time we shall have

$$[(\lambda-1+L)^2+F(\lambda+1)^2](\lambda-1)+(\lambda-1+L)\lambda 2A=0 \ . \qquad (2.29)$$

In the case of the second degree operator

$$L = \frac{4K\Delta t}{d^2}(1-\cos X\cos Y) \ ,$$

while

$$L = \frac{16K'\Delta t}{d^4}(1-\cos X\cos Y)^2 \ ,$$

if the fourth degree operator is used. Let $4K\Delta t/d^2$ be equal to .0057096 and let all other parameters except w have the same values as before. This would correspond to a rather modest value of the diffusion coefficient $K=10^5$ m^2 s^{-1} for the grid size of about 180 km. Concerning the diffusion coefficient corresponding to the fourth degree scheme, we choose

$$K' = \frac{1}{8} 2d^2 K$$

Then the second and fourth degree diffusion terms will give the same rate of velocity change in the case of the two-grid-interval wave.

Again, we shall assume that the real and positive root of (2.29) corresponds to the geostrophic solution. The values of the amplification factor of the geostrophic mode are shown in Figs. 2.11 and 2.12 for the second and fourth degree linear diffusion, respectively. As we can see from the figures, at the point $X=\pi$, $Y=0$ we obtain the value $\lambda=1$. By inspection of the system of equations that we have started from, we can see that we have independent solutions for the equations of motion and the continuity equation. These two independent solutions correspond to damped inertial oscillation and the stationary two-grid-interval wave in the height field. The root $\lambda=1$ is associated with the latter one. Otherwise, the geostrophic mode is damped in the entire region of the admissible wave numbers. As one may have expected, the fourth degree scheme is less dissipative and more scale selective.

Comparing Figs. 2.10-2.12 we can see that the modification in the most of the domain yields better results. Namely, the modification damps the geostrophic mode much less intensively in the smaller wave -number range. Moreover, by contrast to the modification, the diffusion terms applied in the equations of motion are ineffective in eliminating the two-grid-interval wave in the height field.

d. A numerical test

To demonstrate the effect of the modification, two comparative 24 hr integrations starting from the 23 August 1975, 00 GMT data were made using the HIBU (Hydrometeorological Institute and Belgrade University) model. The integration domain extended from 35°W to 40°E

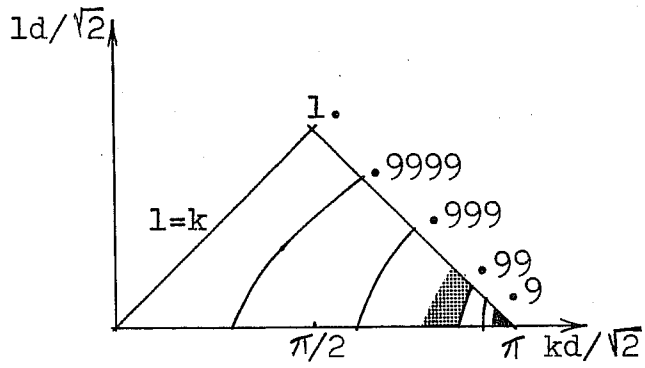

Fig. 2.10. Amplification factor of the geostrophic mode in the case of modified forward-backward scheme. In the lightly shaded area maximum amplification factor is shown. In the heavily shaded area the geostrophic solution does not exist. (After Vasiljević, 1982)

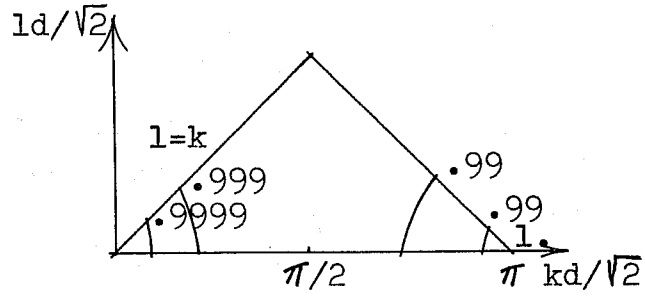

Fig. 2.11. Amplification factor of the geostrophic mode in the case of the second degree linear diffusion. (After Vasiljević, 1982)

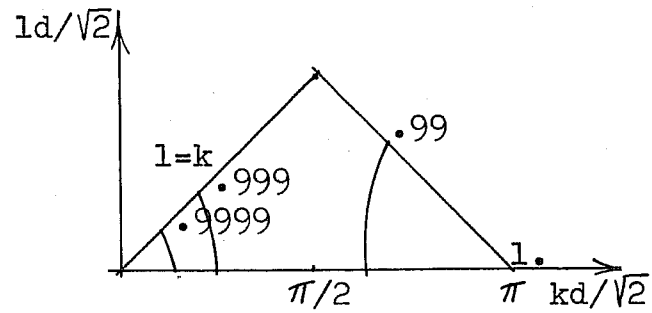

Fig. 2.12. Amplification factor of the geostrophic mode in the case of the fourth degree linear diffusion. (After Vasiljević, 1982)

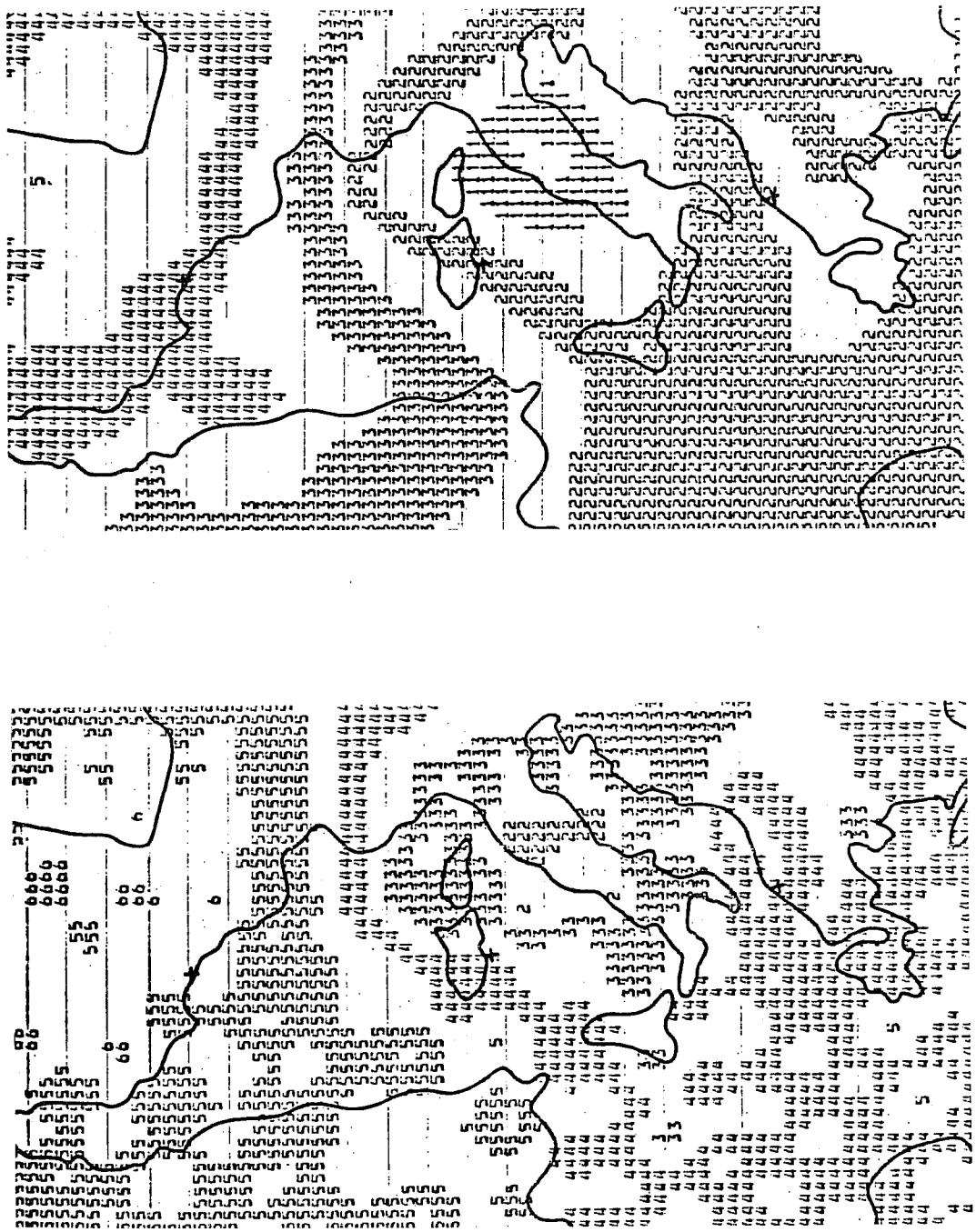

Fig. 2.13. Sea level pressure, 00 GMT 24 August 1975, 24 hr forecast with variable boundary conditions. Above: with w=.25; below: with w=0. (After Janjić, 1979)

and from 30°N to 66°N. A realistic steep topography was included. No lateral diffusion was used in the interior of the integration domain. Only modest lateral diffusion was allowed near the boundaries. The linear diffusion coefficient did not exceed the value which is usually used with the mesh size of 1.5° in the longitudinal and 1° in the latitudinal direction.

The predicted sea level pressure fields are shown in Fig. 2.13. The isolines are situated along the borders of the shaded areas. The shading interval is 2.5 mb. The value of pressure corresponding to the isoline located at the border of the field of fours toward the neighbouring field of threes is 1020 mb.

In contrast to the predicted sea level pressure in the experiment with $w=.25$ shown in Fig. 2.13 (above), the sea level pressure field in the no modification experiment shown in Fig. 2.13 (below) is contaminated by the noise which makes it difficult to recognize the pattern of the significant weather processes. In addition to that, considerably higher values of the sea level pressure are predicted in the no modification experiment in the centre of the cyclone over Italy.

2.5 Computational economy and programming considerations

With equal resolution, i.e., with equal wave-length of the shortest resolvable wave, all rectangular grids require about the same computational effort per time step. Namely, the total number of tendencies of the dependent variables that has to be calculated does not depend on the grid choice. However, on the grids which require more averaging in order to calculate the pressure gradient force and divergence terms, the gravity waves are decelerated, and consequently, longer time steps can be used with the explicit time differencing schemes. Unfortunately, higher economy is thus achieved at the expense of reduced accuracy.

The computational efficiency can be improved by a suitable choice of the time integration scheme. Today, there are two widely accepted procedures offering about the same economy. These are semi-implicit and split-explicit approaches. The former is almost exclusively applied on

the C grid. It should be noted, however, that the economy of the semi-implicit scheme is achieved by decelerating the fastest gravity waves. In this way, some of the favourable features of the C grid with respect to the simulation of the geostrophic adjustment are lost. Also, there is some theoretical evidence that the geostrophic solution left behind will be distorted (Janjić and Wiin-Nielsen, 1977). However, numerical experiments indicate that these effects do not visibly modify the fields obtained in actual integrations.

On the other hand, B and E grids are commonly used in combination with the split-explicit approach based on the forward-backward scheme discussed earlier (Gadd, 1974; 1978; Mesinger, 1974; 1977; Mesinger and Arakawa, 1976; Janjić and Wiin-Nielsen, 1977; Janjić, 1979). On this type of grid trapezoidal time integration scheme can be easily applied for the Coriolis terms.

Another very promising possibility with respect to increasing the efficiency of the calculations has been recently proposed by Bates (1984a; 1984b). In his scheme the semi-Lagrangean approach for the advection terms (Bates and McDonald, 1982) is combined with the alternating-direction-implicit method for the gravity-inertia terms. Successful shallow water equation integrations on the E grid have been reported requiring less than a half of the CPU time needed with the forward-backward scheme.

Concerning programming, it is rather straightforward for all rectangular grids except the E grid. An unpleasant feature of the E grid is that in a limited, rectangular domain, indices of the grid points surrounding the grid point at which the calculation is performed cannot be calculated by simply adding or substracting a constant increment to/from the indices of the current point. Namely, the value of the increment will depend on whether the indices are even or odd. This makes programming for vector machines particularly difficult. However, this problem can be easily eliminated in hemispheric or global models by using indexing as schematically represented in Fig. 2.14.

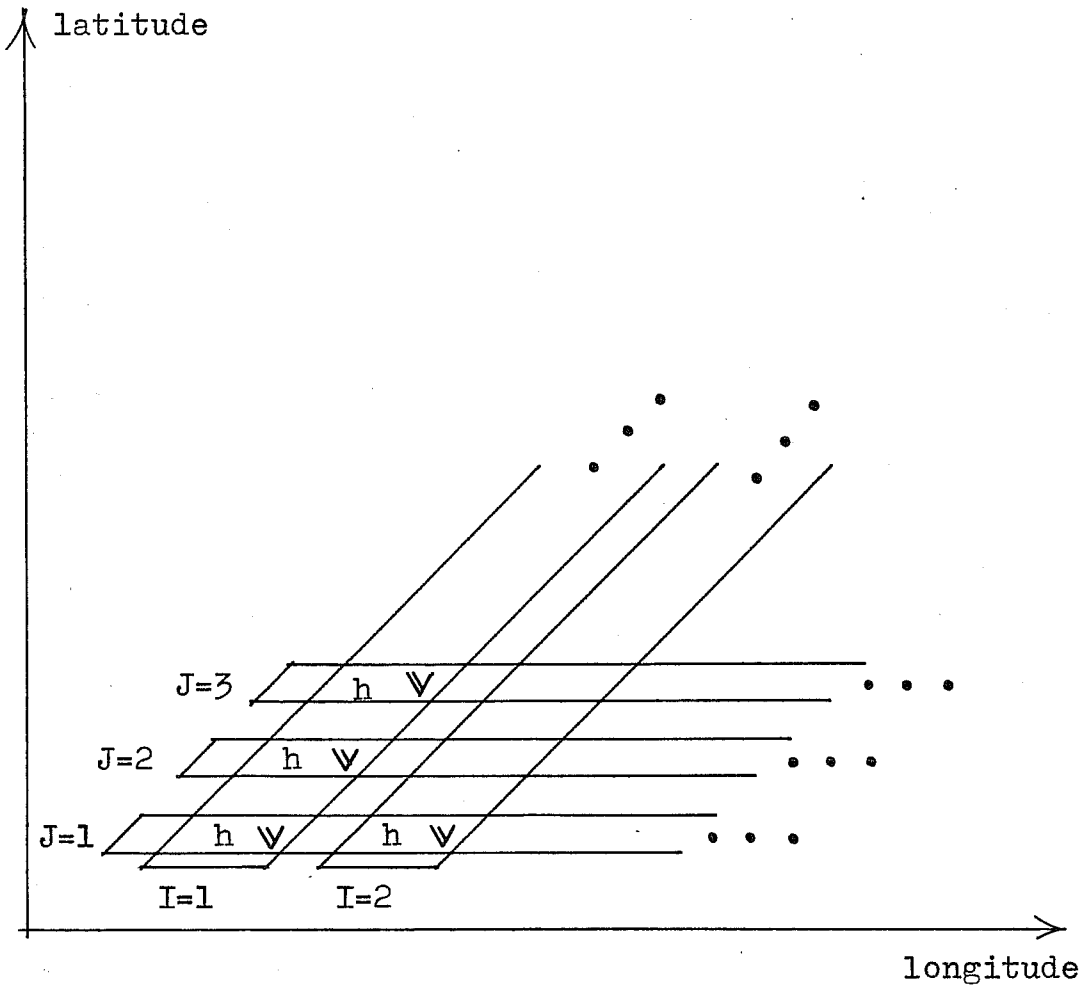

Fig. 2.14. Possible indexing on the E grid in hemispheric or global domains.

3. NON-LINEAR ADVECTION SCHEMES

3.1 General approach and principles

As can be easily verified, it is possible to construct an infinite number of different non-linear advection schemes on any grid type. Thus, the main problem here is again to establish criteria for choosing the most suitable one. We have already discussed some of these, such as local accuracy, stability, phase errors, computational economy. However, all these criteria have been applied within the frame of the linear theory.

A common problem with the non-linear advection schemes is that they erroneously tend to accumulate energy at the smallest resolvable scales. Attacking this problem, Arakawa (1966) proposed that certain important integral properties of the continuous equations be preserved in order to achieve better simulation of the energy spectrum. Being related to the non-linear interactions among various scales, the Arakawa approach falls beyond the limits of the linear theory. In this way a sound theoretical basis has been established in the field in which an empirical approach previously dominated.

Following Fjørtoft's (1953) theory, as the integral constraints, Arakawa suggested that energy and enstrophy be conserved in the case of non-divergent flow. The energy conservation seems to be an obvious choice and has been used before. However, concerning the simulation of the energy spectrum of large-scale quasi-two-dimensional atmospheric motion, its relative importance has been challenged by some experimental and theoretical results (e.g. Arakawa, 1966; Arakawa and Lamb, 1977; Sadourny, 1975; Basdevant and Sadourny, 1975). Namely, it appears that the enstrophy conservation is much more important in this respect and, at the same time, it guarantees almost exact conservation of energy.

The Fjørtoft's theory applies to the flow governed by the non-divergent vorticity equation

$$\frac{\partial \zeta}{\partial t} + J(\psi, \zeta) = 0 \quad .$$

Here, J represents the Jacobi operator and Ψ and ζ are streamfunction and vorticity, respectively. Arakawa (1966) discussed a number of finite difference approximations to the Jacobi operator, and found one, J_A, which together with some other properties of the Jacobi operator, conserves energy and enstrophy. Dealing with the primitive equations, however, we have to find such approximations to the momentum advection terms which in the case of non-divergent flow reduce to the equation

$$\frac{\partial \zeta}{\partial t} + J_A(\Psi, \zeta) = 0 \ .$$

Here, ζ is the finite-difference vorticity analogue. However, this is a non-trivial problem which does not have a unique solution. Usually, the trial and error approach is applied leading to a number of different schemes. The conservation properties of the scheme obtained in this way are then proven a posteriori, going back to the finite difference vorticity equation.

Following the pioneering work of Arakawa, a number of energy and enstrophy conserving schemes has been developed for the grids C (Grammeltvedt, 1969; Arakawa - in Arakawa and Lamb, 1977; Sadourny - in Burridge and Haseler, 1977) and E (Janjić, 1977; 1984; Mesinger, 1981). Recently, Arakawa and Lamb (1981) proposed a more elaborated scheme which conserves potential enstrophy and energy. A scheme which conserves potential enstrophy, but not energy, has been earlier designed by Sadourny (1975). In the case of non-divergent flow, however, the Sadourny scheme does not reduce to the Arakawa Jacobian, but rather to its more accurate enstrophy conserving component Jacobian approximation.

Mainly following the paper by Janjić (1984), we shall here examine the properties relevant for the simulation of the non-linear interactions of several representatives of the C grid and E grid momentum advection schemes based on the Arakawa approach. However, in order to do so, we shall first review certain important implications of the definition of the J_A operator.

3.2 General remarks on the Arakawa Jacobian

a. Definition and properties of the Arakawa Jacobian

If two variables, say A and B, are both defined at the grid points of the stencil shown in Fig. 3.1, the Arakawa Jacobian applied at the central point of the stencil has the form

$$J_A(A,B)=\frac{1}{12d^2}\left[(A_1-A_3)(B_2-B_4)-(A_2-A_4)(B_1-B_3)\right.$$
$$+B_2(A_5-A_6)-B_4(A_8-A_7)-B_1(A_5-A_8)+B_3(A_6-A_7) \qquad (3.1)$$
$$\left.+A_1(B_5-B_8)-A_3(B_6-B_7)-A_2(B_5-B_6)+A_4(B_8-B_7)\right]$$

(Arakawa, 1966; Mesinger and Arakawa, 1976). It has been demonstrated by Arakawa (1966) that

$$J_A(A,A)=0 \ , \qquad (3.2)$$

$$J_A(A,B)=-J_A(B,A) \ , \qquad (3.3)$$

$$\overline{J_A(A,B)}=0 \ , \qquad (3.4)$$

$$\overline{AJ_A(A,B)}=0 \ , \qquad (3.5)$$

$$\overline{BJ_A(A,B)}=0 \ . \qquad (3.6)$$

Here the overbar denotes the area mean taken over a domain with cyclic boundary conditions. In addition to that, as can be inferred from the definition (3.1), we may also write

$$\alpha J_A(A,B)=J_A(\alpha A,B)=J_A(A,\alpha B), \ \alpha=\text{const} \ , \qquad (3.7)$$

$$J_A(A+B,C)=J_A(A,C)+J_A(B,C) \ . \qquad (3.8)$$

Yet another important feature of the Arakawa Jacobian can be readily deduced. Namely, as we can see from (3.1), this operator may be formally regarded as a weighted sum of products of the values of its arguments. On the other hand, if ζ is an arbitrary coordinate

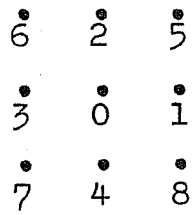

Fig. 3.1. Stencil used to define the Arakawa Jacobian.

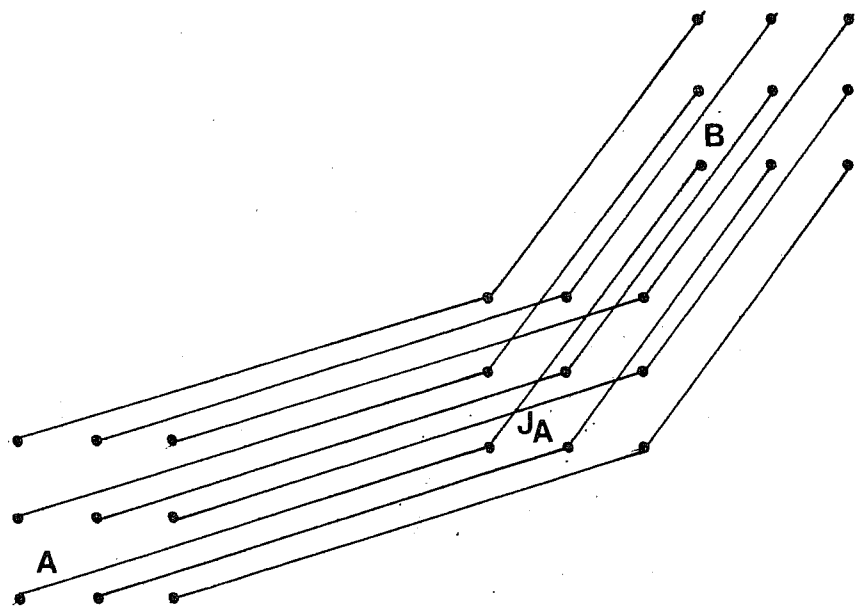

Fig. 3.2. Schematic representation of the application of the Arakawa Jacobian as a more general quadratic form. (After Janjić, 1984)

axis,

$$\delta_\lambda(AB) = \bar{A}^\lambda \delta_\lambda B + \bar{B}^\lambda \delta_\lambda A \ . \tag{3.9}$$

Thus, we may write

$$\delta_\lambda J_A(A,B) = J_A(\bar{A}^\lambda, \delta_\lambda B) + J_A(\delta_\lambda A, \bar{B}^\lambda) \ . \tag{3.10}$$

Finally, as suggested by Janjić (1984), in certain applications it is convenient to consider the Arakawa Jacobian as a more general quadratic form than it is usually done. Namely, normally, both arguments of this operator are defined at each of the nine points of the stencil shown in Fig. 3.1. The J_A operator is then applied at the central point of the stencil. However, a somewhat different situation is also concievable. Namely, let the values of the arguments of J_A , say A and B , be defined on two nine-point stencils which are displaced with respect to each other, and with respect to the nine-point stencil on which the Arakawa Jacobian operates. Prior to the evaluation of the expression (3.1), the values of the arguments are "fetched" from the points of their respective stencils to the points of the stencil associated with the J_A operator. This situation is schematically represented in Fig. 3.2. The thin lines in the figure indicate the "routes of transportation" of the values of the arguments A and B.

To indicate the possibility that the stencils corresponding to the arguments are displaced with respect to each other, we shall use the notation

$$J_A(A_\alpha, B_\beta) \ , \tag{3.11}$$

where the additional subscripts α and β define the locations of the central points of the two stencils. Note that the location at which the expression (3.11) is evaluated is irrelevant and, therefore, we cannot say that the J_A operator applied in this manner is associated with any particular geometrical position.

As we shall see in Section 3.4, the symbols A and B in (3.11) may represent the same physical quantity, such as streamfunction, for

example. However, in contrast to (3.2), because of the displacement, e.g. the expression $J_A(A_\alpha, A_\beta)$ will not be identically equal to zero. A_α and A_β can of course be considered simply as new variables, different from A, defined at the arrival grid points after the displacement has been performed. In this way one can see that the new use of J_A represents merely a more general notation, which introduces no changes in the previously stated properties of J_A.

b. **Arakawa Jacobian as an advection scheme on grids C and E**

In the case of non-divergent flow, to which the Arakawa-Fjørtoft theory applies, the streamfunction is sufficient to describe the wind field. Therefore, if we want to apply the Arakawa Jacobian on a grid used for primitive equations, we have to define the relation between the velocity components and the fields of streamfunction Ψ and velocity potential χ. Namely, consider the distributions of variables $\hat{C}$ and $\hat{E}$ shown in Fig. 3.3. We shall assume that the distance between two nearest grid points carrying the same variable d is the same in both cases. The coordinate systems x',y' and x,y associated with the two grids are also indicated in the figure. The differencing operators along the coordinate axes of these two coordinate systems we define by

$$\delta_\lambda A = \frac{A(\lambda+\Delta\lambda/2) - A(\lambda-\Delta\lambda/2)}{\Delta\lambda} \quad . \tag{3.12}$$

Here, the increment $\Delta\lambda$ takes on the value d or $\sqrt{2}\,d$ depending on whether λ stands for coordinate axes x' and y', or x and y.

Using (3.12) we define the velocity components on the C grid by

$$u' = -\delta_{y'}\Psi + \delta_{x'}\chi, \quad v' = \delta_{x'}\Psi + \delta_{y'}\chi \ , \tag{3.13}$$

and on the E grid by

$$u = -\delta_y\Psi + \delta_x\chi, \quad v = \delta_x\Psi + \delta_y\chi \ . \tag{3.14}$$

With these definitions the grids $\hat{C}$ and $\hat{E}$ viewed in terms of the height and velocity-component points become identical to the grids C and E, respectively.

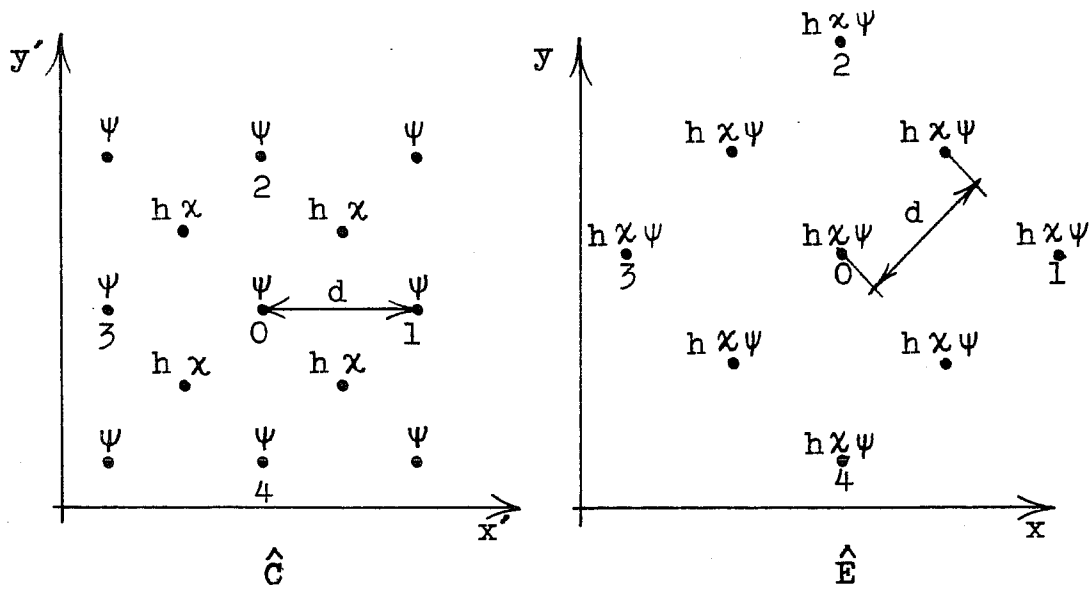

Fig. 3.3. Distributions of variables $\hat{C}$ and $\hat{E}$ with the associated coordinate systems. (After Janjić, 1984)

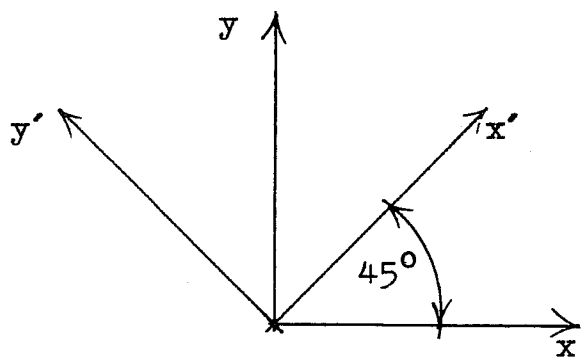

Fig. 3.4. Relative positions of the coordinate systems x',y' and x,y associated with the grids C and E respectively. (After Janjić, 1984).

Having defined the relation between the velocity field and the fields of streamfunction and velocity potential, we shall now turn our attention to a special class of advection schemes. Namely, consider the equation of the form

$$\frac{dZ}{dt} = 0 . \tag{3.15}$$

Here Z is a function of horizontal coordinates and time. If the flow is non-divergent, instead of (3.15) we may write

$$\frac{\partial Z}{\partial t} = -J(\Psi, Z) . \tag{3.16}$$

Seeking a finite-difference advection scheme, we may approximate the Jacobi operator appearing in (3.16) by the Arakawa Jacobian. As has been pointed out, the definition (3.1) requires that both arguments of the Arakawa Jacobian should be defined at the same grid points. However, discretizing the advection equation (3.16) on a given type of grid, we may find that the grid points carrying the streamfunction and the quantity which is being advected do not coincide. To allow for this possibility, replacing the Jacobi operator in (3.16) by the Arakawa Jacobian we shall write

$$\frac{\partial Z}{\partial t} = -J_A(\overline{\Psi}^*, Z) . \tag{3.17}$$

Here, the symbol $\overline{}^*$ denotes a linear averaging operator which is used to define the values of streamfunction at Z grid points. Of course, if Z and Ψ are located at the same points this operator should be ignored.

Prior to their use in primitive equation models, the advection schemes of the form (3.17) must be generalized to include the divergent part of flow. In principle, this can be accomplished by replacing the rotational velocity components by the actual wind (e.g. Arakawa, 1972; Arakawa and Lamb, 1977). However, in order to do so, the rotational velocity components must be present in an explicit form in the expression on the right hand side of (3.17). Depending on whether they have the form of the rotational velocity components in (3.13), or in (3.14), we shall consider the scheme as being defined on the C or on the E grid, respectively.

In this sense, the Arakawa Jacobian is both the C grid and the E grid scheme. To show this, let us assume that the coordinate systems x', y' and x, y are rotated with respect to each other through an angle of 45° as indicated in Fig. 3.4. Furthermore, let a two-point averaging operator be defined by

$$\overline{A}^{\zeta} = \tfrac{1}{2}\left[A(\zeta+\Delta\zeta/2) + A(\zeta-\Delta\zeta/2)\right] , \tag{3.18}$$

where ζ and $\Delta\zeta$ have the same meaning as in (3.12), and, as before, let the repeated application of the operator in the direction of ζ_1 and ζ_2 be denoted by $\overline{}^{\zeta_1,\zeta_2}$. Then, as can be verified by direct inspection, if we replace A and B by $\overline{\Psi}^*$ and Z, respectively, the definition (3.1) can be rearranged to take the form of either of the following two expressions

$$\begin{aligned} J_A(\overline{\Psi}^*, Z) = {} & \tfrac{1}{3}\left\{\delta_x\left[\sqrt{2}\left(-\delta_{y'}\overline{\Psi}^{x'} - \delta_{x'}\overline{\Psi}^{y'}\right)^*\overline{Z}^{x}\right] + \delta_y\left[\sqrt{2}\left(-\delta_{y'}\overline{\Psi}^{x'} + \delta_{x'}\overline{\Psi}^{y'}\right)^*\overline{Z}^{y}\right]\right\} \\ & + \tfrac{2}{3}\left\{\delta_{x'}\left[\left(-\delta_{y'}\overline{\Psi}^{x'y'}\right)^*\overline{Z}^{x'}\right] + \delta_{y'}\left[\left(\delta_{x'}\overline{\Psi}^{x'y'}\right)^*\overline{Z}^{y'}\right]\right\} , \end{aligned} \tag{3.19}$$

$$\begin{aligned} J_A(\overline{\Psi}^*, Z) = {} & \tfrac{1}{3}\left\{\delta_x\left[\left(-\delta_y\Psi\right)^*\overline{Z}^{x}\right] + \delta_y\left[\left(\delta_x\Psi\right)^*\overline{Z}^{y}\right]\right\} \\ & + \tfrac{2}{3}\left\{\delta_{x'}\left[\tfrac{\sqrt{2}}{2}\left(-\delta_y\Psi + \delta_x\Psi\right)^{y'*}\overline{Z}^{x'}\right] + \delta_{y'}\left[\tfrac{\sqrt{2}}{2}\left(\delta_y\Psi + \delta_x\Psi\right)^{x'*}\overline{Z}^{y'}\right]\right\} . \end{aligned} \tag{3.20}$$

Within the brackets on the right hand side of (3.19) we recognize the C grid rotational velocity components as defined in (3.13). Thus, $J_A(\overline{\Psi}^*, Z)$ is indeed a C grid scheme. On the other hand, in (3.20) only the E grid rotational velocity components are present. Therefore, $J_A(\overline{\Psi}^*, Z)$ is an E grid scheme as well.

3.3 Conservation of energy and enstrophy and the non-linear energy cascade on grids C and E

Following a procedure similar to Fjørtoft's(1953), Janjić (1984) examined the impact of the conservation of energy and enstrophy on the grids C and E. Here, we shall present his analysis.

Separating the time derivative of the rotational component of velocity and the contribution of the pure non-divergent part of advection,

the shallow water equations of motion in plane geometry may be written in the form

$$\frac{\partial}{\partial t}\left(-\frac{\partial \Psi}{\partial y}\right) = -J\left(\Psi, -\frac{\partial \Psi}{\partial y}\right) + R \ , \tag{3.21}$$

$$\frac{\partial}{\partial t}\left(\frac{\partial \Psi}{\partial x}\right) = -J\left(\Psi, \frac{\partial \Psi}{\partial x}\right) + S \ . \tag{3.22}$$

To keep the main problem isolated, we have grouped together the terms which are not relevant for our present considerations and denoted them by R and S. For simplicity, we shall assume that the Coriolis parameter is constant.

a. Grid C

On the C grid, the non-divergent advection terms in (3.21) and (3.22) may be approximated using the Arakawa energy and enstrophy conserving scheme (Arakawa and Lamb, 1977), i.e. we may write

$$\frac{\partial}{\partial t}\left(-\delta_{y'} \Psi\right) = -J_A\left(\overline{\Psi}^{y'}, -\delta_{y'} \Psi\right) + R' , \tag{3.23}$$

$$\frac{\partial}{\partial t}\left(\delta_{x'} \Psi\right) = -J_A\left(\overline{\Psi}^{x'}, \delta_{x'} \Psi\right) + S' . \tag{3.24}$$

Using (3.2), (3.3), (3.7), (3.8) and (3.10) together with the identity

$$\frac{d^2}{4}\delta_\Delta(\delta_\Delta A) = \overline{\overline{A}^{\Delta}}^{\Delta} - A \ ,$$

after some algebra, from (3.23) and (3.24) we obtain the vorticity equation of the form

$$\frac{\partial}{\partial t}\left(\nabla_x^2 \Psi\right) = -J_A\left(\Psi, \nabla_x^2 \Psi\right) + \delta_{x'} S' - \delta_{y'} R' \ .$$

Here, using the notation of the grid points introduced on the left hand side of Fig 3.3, the operator ∇_x^2 is defined by

$$\nabla_x^2 \Psi \equiv \delta_{x'}(\delta_{x'} \Psi) + \delta_{y'}(\delta_{y'} \Psi) = \frac{\Psi_1 + \Psi_2 + \Psi_3 + \Psi_4 - 4\Psi_0}{d^2} \tag{3.25}$$

Finally, assuming that the flow is non-divergent, and taking into account that the Coriolis parameter is considered constant, we arrive to the finite-difference approximation to the barotropic non-divergent vorticity

equation

$$\frac{\partial}{\partial t}(\nabla_x^2 \psi) = -J_A(\psi, \nabla_x^2 \psi) . \tag{3.26}$$

From (3.26) we find that due to the properties of the Arakawa Jacobian (3.5) and (3.6),

$$\overline{\psi \frac{\partial}{\partial t} \nabla_x^2 \psi} = 0 \tag{3.27}$$

and

$$\overline{\nabla_x^2 \psi \frac{\partial}{\partial t} \nabla_x^2 \psi} = 0 . \tag{3.28}$$

However,

$$\overline{-A \nabla_x^2 B} = \overline{\delta_{x'} A \delta_{x'} B + \delta_{y'} A \delta_{y'} B} , \tag{3.29}$$

and, therefore, instead of (3.27) we may write

$$\overline{\delta_{y'} \psi \frac{\partial}{\partial t}(\delta_{y'} \psi) + \delta_{x'} \psi \frac{\partial}{\partial t}(\delta_{x'} \psi)} = 0 .$$

Thus, as in the continuous case, the mean kinetic energy

$$K' = \overline{\tfrac{1}{2}[(\delta_{y'} \psi)^2 + (\delta_{x'} \psi)^2]} \tag{3.30}$$

and enstrophy

$$\eta' = \overline{\tfrac{1}{2}(\nabla_x^2 \psi)^2} \tag{3.31}$$

are conserved.

Let us now examine the impact of these conservation properties. For this purpose let us consider the flow in a square domain with cyclic boundary conditions. Let the linear dimensions of the domain be Nd where N is an even integer, and let an expansion of the form

$$\psi = \sum_{m,n} \hat{a}_{mn} e^{i(k'_m x' + l'_n y')} \tag{3.32}$$

be considered inside the domain. Here,

$$m,n = 0, \pm 1, \pm 2, \ldots N/2 \tag{3.33}$$

and the amplitudes $\hat{a}_{mn}$ and $\hat{a}_{-m-n}$ are the complex conjugates of each other. The components of the wave number vector are defined by

$$k'_m = m\frac{2\pi}{Nd} \quad , \quad \ell'_n = n\frac{2\pi}{Nd} \quad . \tag{3.34}$$

Note that the negative values of k' and ℓ' are also allowed. As can be inferred from (3.33) and (3.34), the wave length of the shortest wave present in (3.32) is equal to $2d/\sqrt{2}$. If the wave number vector is oriented in the direction of the coordinate axes, the wave length cannot be smaller than $2d$.

We shall determine the values of the amplitudes $\hat{a}_{mn}$ by requiring that at the Ψ grid points the expression (3.32) takes on the values identical to those of the streamfunction. Then, at any particular grid point

$$\Psi = \sum_{m,n} \hat{a}_{mn} e^{i(k'_m x' + \ell'_n y')} \quad . \tag{3.35}$$

Applying the operator ∇_x^2 to (3.35) we obtain the expansion for vorticity which is analogous to that for the streamfunction, i.e.,

$$\nabla_x^2 \Psi = -\sum_{m,n} \lambda'^2_{mn} \hat{a}_{mn} e^{i(k'_m x' + \ell'_n y')} \quad . \tag{3.36}$$

Here,

$$\lambda'^2_{mn} = \frac{4}{d^2}(\sin^2 k'_m d/2 + \sin^2 \ell'_n d/2) \tag{3.37}$$

are the eignevalues of the finite difference Laplacian (3.25). The values of the non-dimenional function $d^2\lambda'^2_{mn}$ are presented in Fig. 3.5. Since this function is symmetric with respect to the lines $|k'| = |\ell'|$ and k' and ℓ' axes, to avoid repetition, we have restricted ourselves to the triangular domain between the positive k' axis and the line $k' = \ell'$. As can be seen from the figure, λ'^2_{mn} is an increasing function of each of the two wave number components.

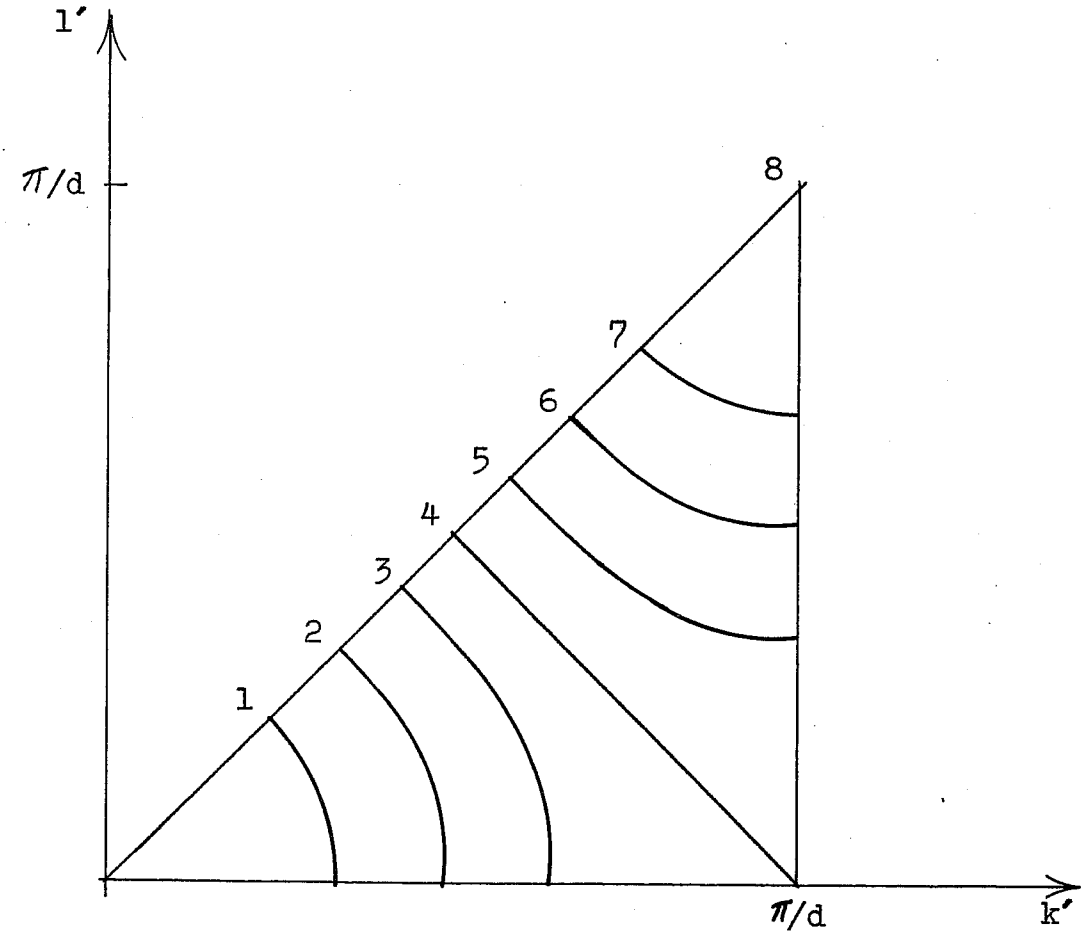

Fig. 3.5. Eigenvalues of the finite-difference Laplacian ∇_x^2. The values are non-dimensionalized by multiplication by d^2. (After Janjić, 1984)

As in the continuous case, we can now express the mean kinetic energy and enstrophy in terms of the amplitudes $\hat{a}_{mn}$ and the eigenvalues λ'^2_{mn} . Namely, using (3.29) we may write

$$K' = -\overline{\tfrac{1}{2}\psi\nabla_x^2\psi} \ . \tag{3.38}$$

Substituting (3.35) and (3.36) into (3.38) we obtain

$$K' = \tfrac{1}{2}\sum_{p,q,r,s} \lambda'^2_{rs}\,\hat{a}_{rs}\,\hat{a}_{pq}\,\overline{e^{i[(k'_p+k'_r)x'+(l'_q+l'_s)y']}} \ . \tag{3.39}$$

As in the continuous case, we can further simplify the expression on the right hand side of this formula. Namely, note that even if $(k'_p + k'_r)$ and $(l'_q + l'_s)$ exceed the maximum allowed wave numbers, due to aliasing they will be misinterpreted by the grid as if they belong to the admissible wave number range. Therefore, this particular case does not require separate consideration. Also, it can be verified in a straightfroward manner that the grid point values of the considered exponential function and its averages over the C grid grid-box area are related by

$$\overline{e^{i(k'x'+l'y')}} = \frac{k'\frac{d}{2}}{\sin k'\frac{d}{2}}\ \frac{l'\frac{d}{2}}{\sin l'\frac{d}{2}}\ \frac{1}{d^2}\int_{y'-\frac{d}{2}}^{y'+\frac{d}{2}}\int_{x'-\frac{d}{2}}^{x'+\frac{d}{2}} e^{i(k'x'+l'y')}\,dx'dy'$$

and consequently

$$\overline{e^{i(k'x'+l'y')}} = \frac{k'\frac{d}{2}}{\sin k'\frac{d}{2}}\ \frac{l'\frac{d}{2}}{\sin l'\frac{d}{2}}\ \frac{1}{N^2d^2}\int_{-N\frac{d}{2}}^{N\frac{d}{2}}\int_{-N\frac{d}{2}}^{N\frac{d}{2}} e^{i(k'x'+l'y')}\,dx'dy' \ . \tag{3.40}$$

Taking into account that we have prescribed the cyclic boundary conditions, from (3.40) we obtain that, unless $k'=0$ and $l'=0$,

$$\overline{e^{i(k'x'+l'y')}} = 0 \ .$$

Thus, the only terms which remain on the right hand side of (3.39) are those corresponding to the case $p=-r$, $q=-s$. Then the exponent vanishes and the amplitudes $\hat{a}_{rs}$ and $\hat{a}_{pq}$ are complex conjugates of each other.

Thus,

$$K' = \tfrac{1}{2} \sum_{m,n} \lambda'^2_{mn} |\hat{a}_{mn}|^2 \ . \qquad (3.41)$$

Analogously, for the mean enstrophy we obtain

$$\eta' = \tfrac{1}{2} \sum_{m,n} \lambda'^4_{mn} |\hat{a}_{mn}|^2 \ . \qquad (3.42)$$

In analogy with considerations that have been done in the continuous case, we shall rewrite (3.41) and (3.42) in the form

$$K' = \sum_{p}^{P} K'_p \ , \qquad (3.43)$$

$$\eta' = \sum_{p}^{P} \lambda'^2_p K'_p \ . \qquad (3.44)$$

Here, the kinetic energy and enstrophy contributions have been reordered in the ascending order of the eigenvalues. The multiple eigenvalues have been assigned the same subscript p, and the energies K'_p are defined by

$$K'_p = \sum_{\lambda'^2_{mn} = \lambda'^2_p} \lambda'^2_{mn} |\hat{a}_{mn}|^2 \ , \qquad (3.45)$$

i.e., K'_p is the total energy associated with the scales defined by λ'^2_p. The symbol P denotes the total number of different values that the eigenvalues take. Comparing (3.43) and (3.44) with the corresponding formulae for the continuous case (Fjørtoft, 1953), we can see that this time the sums (3.43) and (3.44) are finite and the eigenvalues (3.37) increase slower with increasing wave numbers. Note that the slower increase of the eigenvalues means that more energy is allowed at smaller scales. As a further difference, one may note that the meaning of the eigenvalues λ'^2_p has to some extent changed. Namely, since the contours of λ'^2_p (Fig. 3.5) are not circles of constant values of the two-dimensional wave number, a given scale, defined by the intensity of the wave-number vector, now is not associated with a single value of λ'_p. Instead, it spreads over a range of values of λ'_p, the extent of this range depending on how much the contours differ from the circular shape. In other respects, full analogy is preserved. Thus, if energy and enstrophy are conserved, the non-linear rotational energy cascade on the

C grid will be subject to similar limitations as in the continuous case.

b. Grid E

As can be inferred from the definitions (3.13), (3.14) and (3.25), the C grid rotational energy (3.30) and enstrophy (3.31) cannot be calculated directly from the velocity components on the E grid. The definition of E-grid velocity components (3.14) leads to different definitions of energy and enstrophy and, therefore, we may expect that the conservation of these two quantities will not have the same meaning as in the case of the grid C.

A non-divergent advection scheme conserving energy and enstrophy on the E grid can be designed by analogy with the scheme (3.23)-(3.24). Namely, we may write

$$\frac{\partial}{\partial t}(-\delta_y \Psi) = -J_A(\overline{\Psi}^y, -\delta_y \Psi) + R \quad , \tag{3.46}$$

$$\frac{\partial}{\partial t}(\delta_x \Psi) = -J_A(\overline{\Psi}^x, \delta_x \Psi) + S \quad . \tag{3.47}$$

Similarly as before, in the case of non-divergent flow, from (3.46) and (3.47) we obtain

$$\frac{\partial}{\partial t}(\nabla_+^2 \Psi) = -J_A(\Psi, \nabla_+^2 \Psi) \quad , \tag{3.48}$$

where, using the notation of the grid points introduced on the right hand side of Fig. 3.3, the operator ∇_+^2 is defined by

$$\nabla_+^2 \Psi \equiv \delta_x(\delta_x \Psi) + \delta_y(\delta_y \Psi) = \frac{\Psi_1 + \Psi_2 + \Psi_3 + \Psi_4 - 4\Psi_0}{2d^2} \quad . \tag{3.49}$$

As before, using (3.5) and (3.6), from (3.48) it follows that the mean kinetic energy

$$K = \overline{\tfrac{1}{2}[(\delta_y \Psi)^2 + (\delta_x \Psi)^2]} = -\overline{\tfrac{1}{2} \Psi \nabla_+^2 \Psi} \quad , \tag{3.50}$$

and the mean enstrophy

$$\eta = \overline{\tfrac{1}{2}(\nabla_+^2 \Psi)^2} \quad , \tag{3.51}$$

are conserved.

Further examples of the E grid energy and enstrophy conserving schemes which reduce to the form (3.48) in the case of non-divergent flow are those discussed by Janjić (1977) and Mesinger (1981).

Comparing (3.48) and (3.26) we can see that the only difference is the definition of vorticity. However, it will be demonstrated shortly that this difference may profoundly affect the non-linear energy cascade simulation. Namely, let us again consider the flow in a square domain with cyclic boundary conditions. Let the linear dimensions of the domain be $Jd/\sqrt{2}$, where J is an even integer. For the streamfunction we shall use the representation analogous to (3.35). Namely, we shall assume that at any grid point the value of the streamfunction can be calculated from the formula

$$\psi = \sum_{m,n} \hat{a}_{mn} e^{i(k_m x + \ell_n y)} , \qquad (3.52)$$

where m and n are integers and

$$|m| + |n| \leq J/2 .$$

This time the components of the wave-number vector are defined by

$$k_m = m \frac{2\pi}{Jd/\sqrt{2}} , \quad \ell_n = n \frac{2\pi}{Jd/\sqrt{2}} .$$

The amplitudes $\hat{a}_{mn}$ and $\hat{a}_{-m-n}$ are again complex conjugates of each other. They are determined from the requirement that the formula (3.52) should be valid for a given streamfunction field.

An analogous expansion for vorticity we obtain by applying the operator ∇_+^2 to (3.52). In this way we find that

$$\nabla_+^2 \psi = - \sum_{m,n} \lambda_{mn}^2 \hat{a}_{mn} e^{i(k_m x + \ell_n y)} , \qquad (3.53)$$

where the eigenvalues of the finite-difference Laplacian ∇_+^2 are defined by

$$\lambda_{mn}^2 = \frac{2}{d^2} \left(\sin^2 k_m \frac{d}{\sqrt{2}} + \sin^2 \ell_n \frac{d}{\sqrt{2}} \right) . \qquad (3.54)$$

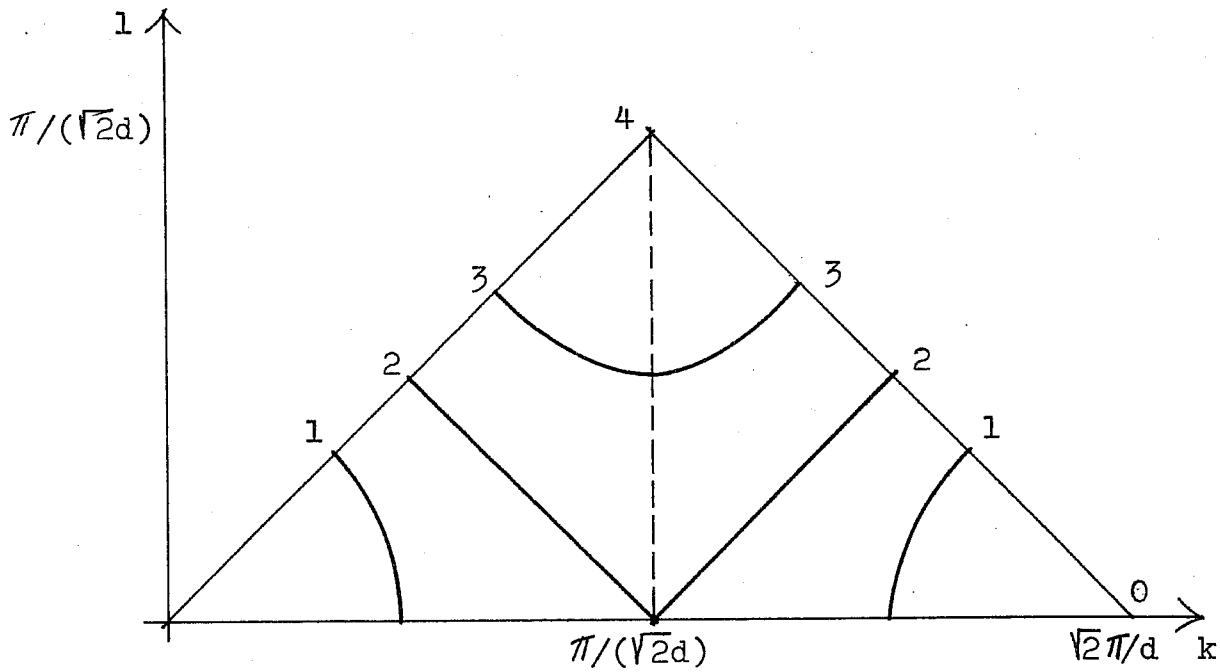

Fig. 3.6. Eigenvalues of the finite-difference Laplacian ∇_4^2. The values are non-dimenionalized by multiplication by d^2. (After Janjić, 1984)

The values of the non-dimenional function $d^2\lambda^2_{mn}$ are presented in Fig. 3.6. Since this function is symmetric with respect to the lines $|k| = |\ell|$ and k and ℓ axes, to avoid repetition, we have restricted ourselves to the triangular domain in between the positive k axis and the line $k = \ell$. Within this domain, however, there is an additional axis of symmetry, the line $k = \pi/\sqrt{2}d$. As we can see from the figure, the values of the function (3.54) to the left of this axis have their exact counterparts to the right of it. At the same time, while to the left of this axis the eigenvalues generally increase with increasing intensity of the wave-number vector, the opposite is true in the rest of the diagram. This is fundamentally different from the situation on the C grid.

Similarly as before, substituting (3.52) and (3.53) into (3.50) and (3.51), we find that the mean kinetic energy K and enstrophy η may be written in the form

$$K = \tfrac{1}{2} \sum_{m,n} \lambda^2_{mn} |\hat{a}_{mn}|^2 \quad , \tag{3.55}$$

$$\eta = \tfrac{1}{2} \sum_{m,n} \lambda^4_{mn} |\hat{a}_{mn}|^2 \quad . \tag{3.56}$$

As in the case of the C grid, here we have used a formula stating that the integral over a grid box of an exponential function of the form

$$e^{i(kx+\ell y)} \tag{3.57}$$

is proportional to the value of the function in the middle of the grid box. Of course, it is possible that due to multiplications in (3.50) and (3.51), the wave-numbers k and ℓ in (3.57) exceed the maximum allowed ones. However, again they will be misinterpreted by the grid as if they belong to the admissible wave-number range. Therefore, the relation between the value of the function (3.57) in the middle of a grid box, and its integral over the grid box, will remain the same in this special case as well.

Defining

$$K_{mn} \equiv \tfrac{1}{2} \lambda^2_{mn} |\hat{a}_{mn}|^2 \quad , \tag{3.58}$$

instead of (3.55) and (3.56) we may write

$$K = \sum_{m,n} K_{mn} \quad , \tag{3.59}$$

$$\eta = \sum_{m,n} \lambda^2_{mn} K_{mn} \quad . \tag{3.60}$$

Similarly as before, only the magnitudes of λ^2_{mn} are relevant for the purpose of our analysis. Thus, instead of (3.59) and (3.60) we shall write

$$K = \sum_{p}^{P-1} K_p = \text{const} \quad , \tag{3.61}$$

$$\eta = \sum_{p}^{P-1} \lambda^2_p K_p = \text{const} \quad . \tag{3.62}$$

Here, we have reordered the kinetic energy and enstrophy contributions in the ascending order of the eigenvalues in the area where they generally increase with increasing intensity of the wave-number vector, i.e., for $|k_m| \leq \pi/(\sqrt{2}d)$ and $|l_n| \leq \pi/(\sqrt{2}d)$; and in the descending order in the remaining area, where the reverse is true. The same subscript has been assigned to contributions associated with multiple eigenvalues within a single one of the two areas. The symbol P denotes the total number of contributions resulting from the described reordering. Finally, K_p is the sum of energies associated, through this reordering, with a single subscript. It should be noted that there can be no rotational energy in the sense of formula (3.58) at the very shortest resolvable scales. Namely, according to (3.54), the corresponding eigenvalue is equal to zero. For this reason, the subscript p does not exceed $P-1$ in (3.61) and (3.62).

Inspecting the formulae (3.61) and (3.62), and the corresponding formulae for the C grid, (3.43) and (3.44), we can see that the situation is now fundamentally different. Namely, since the eigenvalues λ_p take on same values in both the large and small scale ranges, an unlimited exchange of energy between these two ranges is possible without violation of the constraints (3.61) and (3.62). Thus, the conservation of energy and enstrophy as defined on the E grid does not guarantee that there can be no systematic transport of energy towards smaller scales.

3.4 Advection scheme for semi-staggered grid with controlled non-linear energy cascade

a. Derivation of the scheme

As we have seen, the conservation of energy and enstrophy on semi-staggered grids cannot provide efficient control over the non-linear energy cascade. Instead, Janjić (1984) suggested that energy and enstrophy as defined on the staggered grid C be conserved. Here, we shall present his derivation of an E grid scheme starting from the C grid scheme (3.23)-(3.24). Being simply the transformed C grid scheme, the Janjić scheme will also conserve the C-grid energy (3.30) and enstrophy (3.31).

Deriving the new scheme we shall again assume that the coordinate systems x',y' and x,y, associated with the grids C and E respectively, are rotated with respect to each other as indicated in Fig. 3.4. This rotation, we furthermore assume, is performed with both coordinate origins at Ψ points, so that after the rotation, the Ψ points of the two grids coincide. Thus, after some algebra, from (3.23) and (3.24) we obtain

$$\frac{\partial}{\partial t}(-\delta_y \Psi) = -\frac{\sqrt{2}}{2}\left[\overline{J_A(\overline{\Psi}^{y'}, -\delta_{y'}\Psi)}^{x'} - \overline{J_A(\overline{\Psi}^{x'}, \delta_{x'}\Psi)}^{y'}\right] + \frac{\sqrt{2}}{2}\left(\overline{R'}^{x'} - \overline{S'}^{y'}\right) \qquad (3.63)$$

$$\frac{\partial}{\partial t}(\delta_x \Psi) = -\frac{\sqrt{2}}{2}\left[\overline{J_A(\overline{\Psi}^{y'}, -\delta_{y'}\Psi)}^{x'} + \overline{J_A(\overline{\Psi}^{x'}, \delta_{x'}\Psi)}^{y'}\right] + \frac{\sqrt{2}}{2}\left(\overline{R'}^{x'} + \overline{S'}^{y'}\right) . \qquad (3.64)$$

On the left hand sides of (3.63) and (3.64) we recognize the time derivatives of the E grid non-divergent velocity components.

The remaining, more difficult problem is to transform the non-divergent advection terms. Namely, in (3.63) and (3.64) these terms are calculated using the C grid velocity components. On the E grid, they must be expressed in terms of the E-grid rotational wind. However, due to non-linearity of the operators, this cannot be done in a straightforward manner.

Let us first examine the advection term on the right hand side

of (3.63). Using the notation introduced in Fig. 3.7, at the point 0,

$$-\frac{\sqrt{2}}{2}\left[J_A(\overline{\Psi}^{y'}_{,}-\delta_{y'}\Psi)-J_A(\overline{\Psi}^{x'}_{,}\delta_{x'}\Psi)\right]=$$

$$=-\frac{\sqrt{2}}{4}\left[J_A(\overline{\Psi}^{y'}_{,}-\delta_{y'}\Psi)_1+J_A(\overline{\Psi}^{y'}_{,}-\delta_{y'}\Psi)_3-J_A(\overline{\Psi}^{x'}_{,}\delta_{x'}\Psi)_2-J_A(\overline{\Psi}^{x'}_{,}\delta_{x'}\Psi)_4\right]. \tag{3.65}$$

The first term in the square brackets on the right hand side of (3.65) may be rewritten in the form

$$J_A(\overline{\Psi}^{y'}_{,}-\delta_{y'}\Psi)_1=J_A\left(\frac{\Psi_6+\Psi_5}{2},\frac{\Psi_6-\Psi_5}{d}\right).$$

Here, the combination of additional subscripts 5 and 6 indicates the central points of the nine-point stencils corresponding to each of the two arguments. In this case the two stencils coincide, their central points being located in between the points 5 and 6, i.e. at the point 1. Having in mind (3.7) and (3.8), and taking advantage of the notation (3.11), we may further write

$$J_A(\overline{\Psi}^{y'}_{,}-\delta_{y'}\Psi)_1=\frac{1}{2d}\left[J_A(\Psi_6,\Psi_6)-J_A(\Psi_6,\Psi_5)+J_A(\Psi_5,\Psi_6)-J_A(\Psi_5,\Psi_5)\right].$$

However, due to the properties of the Arakawa Jacobian (3.2) and (3.3), which, as stated, are not modified by the present more general notation, the first and the last term in the square brackets must vanish, and the remaining two terms with displaced arguments may be written as

$$J_A(\overline{\Psi}^{y'}_{,}-\delta_{y'}\Psi)_1=\frac{1}{d}J_A(\Psi_5,\Psi_6)=-\frac{1}{d}J_A(\Psi_6,\Psi_5). \tag{3.66}$$

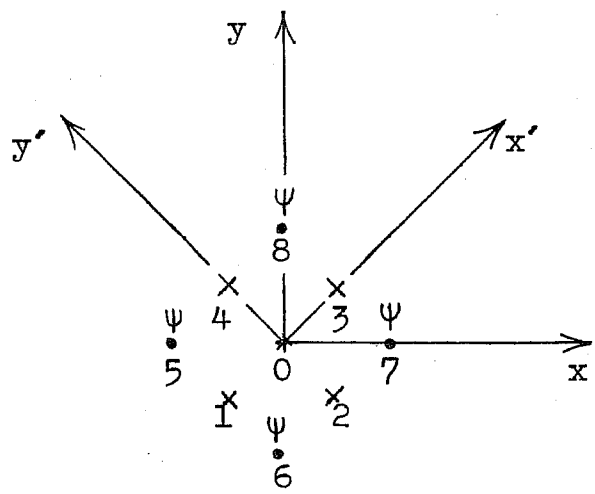

Fig. 3.7. Notation of grid points and coordinate systems used to derive the E grid scheme which conserves energy and enstrophy as defined on the C grid. (After Janjić, 1984)

An analogous procedure applied to the remining three terms in square brackets on the right hand side of (3.65) yields

$$J_A(\overline{\Psi}^{y'}, -\delta_{y'}\Psi)_3 = \frac{1}{d} J_A(\Psi_8, \Psi_7) = -\frac{1}{d} J_A(\Psi_7, \Psi_8) , \tag{3.67}$$

$$J_A(\overline{\Psi}^{x'}, \delta_{x'}\Psi)_2 = \frac{1}{d} J_A(\Psi_6, \Psi_7) = -\frac{1}{d} J_A(\Psi_7, \Psi_6) , \tag{3.68}$$

$$J_A(\overline{\Psi}^{x'}, \delta_{x'}\Psi)_4 = \frac{1}{d} J_A(\Psi_5, \Psi_8) = -\frac{1}{d} J_A(\Psi_8, \Psi_5) . \tag{3.69}$$

Combining (3.66) and (3.69) we obtain

$$J_A(\overline{\Psi}^{y'}, -\delta_{y'}\Psi)_1 - J_A(\overline{\Psi}^{x'}, \delta_{x'}\Psi)_4 = \frac{1}{d} J_A(\Psi_5, \Psi_6 - \Psi_8) . \tag{3.70}$$

Similarly, from (3.67) and (3.68) we find that

$$J_A(\overline{\Psi}^{y'}, -\delta_{y'}\Psi)_3 - J_A(\overline{\Psi}^{x'}, \delta_{x'}\Psi)_2 = \frac{1}{d} J_A(\Psi_7, \Psi_6 - \Psi_8) . \tag{3.71}$$

Substituting (3.70) and (3.71) into (3.65) we arrive to the formula

$$-\frac{\sqrt{2}}{4}\left[J_A(\overline{\Psi}^{y'}, -\delta_{y'}\Psi)_1 + J_A(\overline{\Psi}^{y'}, -\delta_{y'}\Psi)_3 - J_A(\overline{\Psi}^{x'}, \delta_{x'}\Psi)_2 - J_A(\overline{\Psi}^{x'}, \delta_{x'}\Psi)_4\right] = -J_A\left(\frac{\Psi_5 + \Psi_7}{2}, \frac{\Psi_6 - \Psi_8}{\sqrt{2}\, d}\right) . \tag{3.72}$$

As can be seen from Fig. 3.7, the arguments of J_A on the right hand side of (3.72) are defined on the same stencil, its central point being located at the point zero. Therefore, we can again use the usual notation. Thus, generalizing the result (3.72), we may write

$$\frac{\partial}{\partial t}(-\delta_y \Psi) = -J_A(\overline{\Psi}^{x}, -\delta_y \Psi) + \frac{\sqrt{2}}{2}(\overline{R'}^{x'} - \overline{S'}^{y'}) . \tag{3.73}$$

Starting from (3.64), an analogous procedure would lead to the scheme

$$\frac{\partial}{\partial t}(\delta_x \Psi) = -J_A(\overline{\Psi}^{y}, \delta_x \Psi) + \frac{\sqrt{2}}{2}(\overline{R'}^{x'} + \overline{S'}^{y'}) . \tag{3.74}$$

Under the J_A operator sign on the right hand sides of (3.73) and (3.74) we recognize the E-grid rotational velocity components as the quantities which are being advected by the non-divergent wind. Thus, having in mind the E-grid representation of the Arakawa Jacobian (3.20), we find that we have arrived to an E-grid non-divergent advection scheme. Since

this scheme is only a transformation of the scheme (3.63)-(3.64), it will conserve the C-grid energy and enstrophy. In addition to that, due to the properties of the Arakawa Jacobian (3.6) and (3.4), the scheme will conserve the rotational E-grid energy and momentum.

It is interesting to note that the E-grid equivalent of the Arakawa (1972) B-grid non-divergent advection scheme is the arithmetic mean of the schemes (3.46)-(3.47) and (3.73)-(3.74).

So far we have not discussed the terms R' and S' appearing in (3.73) and (3.74). Apparently, we must use independently developed schemes for these terms which better fit the E-grid structure. By doing so we cannot alter the favourable features of the non-divergent advection scheme.

b. Properties of the scheme

Following Janjić (1984), let us now examine the restrictions imposed upon the non-linear cascade of the E-grid rotational energy by the C-grid enstrophy conservation. In order to do so, note that due to different orientation of the coordinate axes, the eigenvalues of the finite-difference Laplacian (3.25) on the E grid take the form

$$\lambda'^2_{mn} = \frac{4}{d^2}\left(1 - \cos k_m \frac{d}{\sqrt{2}} \cos l_n \frac{d}{\sqrt{2}}\right) .$$

Thus, from (3.42) we find that in the x,y coordinate system associated with the E grid

$$\eta' = \frac{1}{2}\sum_{m,n}\left[\frac{4}{d^2}\left(1-\cos k_m \frac{d}{\sqrt{2}}\cos l_n \frac{d}{\sqrt{2}}\right)\right]^2 |\hat{a}_{mn}|^2 .$$

Taking into account (3.54) and (3.58), we shall rewrite this formula in the form

$$\eta' = \sum_{m,n} \Lambda^2_{mn} K_{mn}$$

where

$$\Lambda^2_{mn} = \frac{\lambda'^4_{mn}}{\lambda^2_{mn}} = \frac{8}{d^2}\,\frac{\left(1 - \cos k_m \frac{d}{\sqrt{2}} \cos l_n \frac{d}{\sqrt{2}}\right)}{\sin^2 k_m \frac{d}{\sqrt{2}} + \sin^2 l_n \frac{d}{\sqrt{2}}} . \qquad (3.75)$$

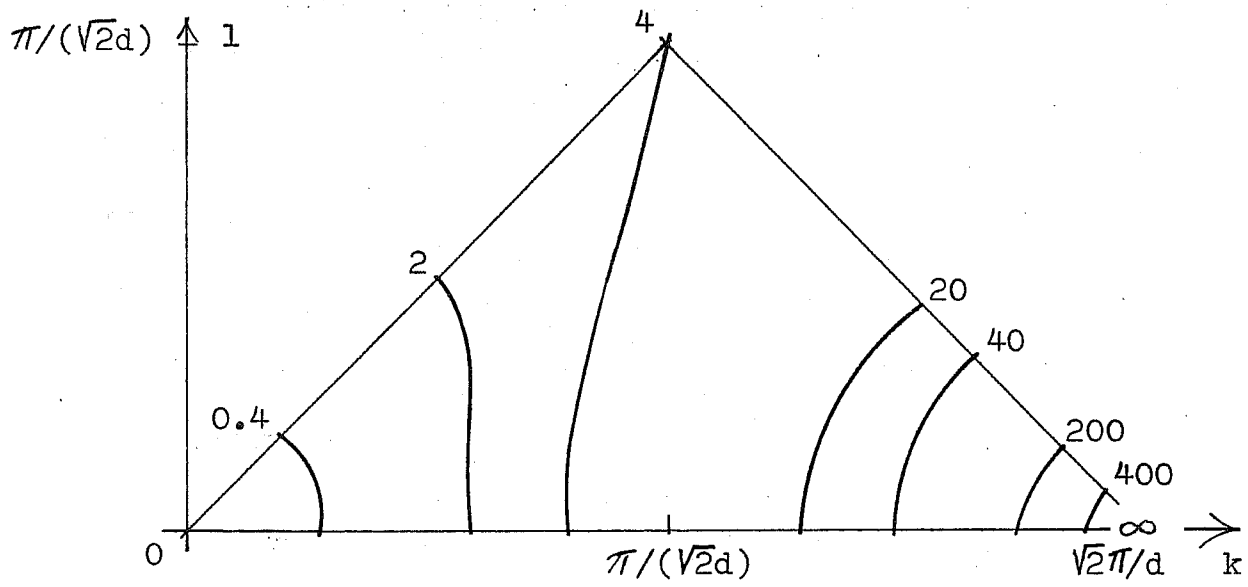

Fig. 3.8. The analogues of the eigenvalues of a finite-difference Laplacian for a scheme which conserves E-grid energy and C-grid enstrophy. The values are non-dimenionalized by multiplication by d^2. (After Janjić, 1984)

he non-dimensional function $d^2\Lambda^2_{mn}$ is presented in Fig. 3.8. To avoid epetition, we have again restricted ourselves to the triangular domain n between the positive k axis and the line $k=l$. As can be seen from he figure, this time the "eigenvalues" (3.75) generally increase with ncreasing intensity of the wave number vector, and even tend to infinity. his singularity reflects the fact that there can be no E-grid rotational nergy at the shortest resolvable scale. Comparison of Figs. 3.5, 3.6 nd 3.8 reveals that the amount of energy which can be transported to he short-wave range is subject to much severer restriction than it was he case with the other energy and enstrophy conserving schemes.

. Generalization of the scheme to include the divergent part of flow

Following a procedure similar to that of Arakawa and Lamb (1977), anjić (1984) derived the approximations to the advection terms of the

shallow water equations which in the case of non-divergent flow reduce to the scheme (3.73)-(3.74), and analyzed the conservation properties of the scheme thus obtained. Here, we shall reproduce his results.

Multiplying, e.g., (3.73) by the height of the free surface, which for a while we shall assume to be constant, and taking into account the definition (3.20), we may write

$$hJ_A(\overline{\psi}^x, -\delta_y\psi) = \frac{1}{3}\{\delta_x[\overline{\overline{h}^x(-\delta_y\psi)}^x\,\overline{(-\delta_y\psi)}^x] + \delta_y[\overline{\overline{h}^y(\delta_x\psi)}^x\,\overline{(-\delta_y\psi)}^y]\}$$
$$+ \frac{2}{3}\{\delta_{x'}[\overline{\overline{h}^{x'}\overline{\tfrac{\sqrt{2}}{2}(-\delta_y\psi+\delta_x\psi)}^{y'}}^x\,\overline{(-\delta_y\psi)}^{x'}] + \delta_{y'}[\overline{\overline{h}^{y'}\overline{\tfrac{\sqrt{2}}{2}(\delta_y\psi+\delta_x\psi)}^{x'}}^x\,\overline{(-\delta_y\psi)}^{y'}]\}\,. \tag{3.76}$$

If we define the mass fluxes in the directions of the coordinate axes x, y, x′, y′ by

$$\begin{aligned} U &= \overline{h}^x u\,, \\ V &= \overline{h}^y v\,, \\ U' &= \overline{h}^{x'}\tfrac{\sqrt{2}}{2}(u+v)\,, \\ V' &= \overline{h}^{y'}\tfrac{\sqrt{2}}{2}(-u+v)\,, \end{aligned} \tag{3.77}$$

and replace the non-divergent velocity components by u and v, respectively, instead of the expression on the right hand side of (3.76) we obtain

$$\frac{1}{3}[\delta_x(\overline{U}^x\overline{u}^x) + \delta_y(\overline{V}^x\overline{u}^y)] + \frac{2}{3}[\delta_{x'}(\overline{U'}^x\overline{u}^{x'}) + \delta_{y'}(\overline{V'}^x\overline{u}^{y'})]\,. \tag{3.78}$$

Using this "isotropic" approximation we may write

$$\frac{\partial}{\partial t}(h_u u) = -\{\frac{1}{3}[\delta_x(\overline{U}^x\overline{u}^x) + \delta_y(\overline{V}^x\overline{u}^y)] + \frac{2}{3}[\delta_{x'}(\overline{U'}^x\overline{u}^{x'}) + \delta_{y'}(\overline{V'}^x\overline{u}^{y'})]\} + \ldots \tag{3.79}$$

Here, we have written explicitly only the flux form advection term. The remaining terms represented by dots are not interesting for our present considerations. The symbol h_u denotes yet undefined value of h at u points. With the aid of the identity

$$\delta_s(B\overline{A}^s) = A\delta_s B + \overline{B\delta_s A}^s\,,$$

where λ is an arbitrary coordinate axis, (3.79) can be further transformed to take the form

$$h_u \frac{\partial u}{\partial t} + u \frac{\partial h_u}{\partial t} = -\left[\frac{1}{3}\left(\overline{\overline{U}^x \delta_x u}^x + \overline{\overline{V}^x \delta_y u}^y\right) + \frac{2}{3}\left(\overline{\overline{U'}^x \delta_{x'} u}^{x'} + \overline{\overline{V'}^x \delta_{y'} u}^{y'}\right)\right]$$
$$-\overline{\left[\frac{1}{3}\left(\delta_x U + \delta_y V\right) + \frac{2}{3}\left(\delta_{x'} U' + \delta_{y'} V'\right)\right]}^x + \ldots \qquad (3.80)$$

We have now arrived at the point where we have to specify the continuity equation approximation. Having defined the mass fluxes by (3.77), it is natural to choose the "isotropic" form

$$\frac{\partial h}{\partial t} = -\left[\frac{1}{3}\left(\delta_x U + \delta_y V\right) + \frac{2}{3}\left(\delta_{x'} U' + \delta_{y'} V'\right)\right] . \qquad (3.81)$$

Comparing (3.80) and (3.81), we find that we must require that

$$h_u = \overline{h}^x .$$

With this definition of h_u we obtain the advection scheme for the u component of the form

$$\frac{\partial u}{\partial t} = -\frac{1}{\overline{h}^x}\left[\frac{1}{3}\left(\overline{\overline{U}^x \delta_x u}^x + \overline{\overline{V}^x \delta_y u}^y\right) + \frac{2}{3}\left(\overline{\overline{U'}^x \delta_{x'} u}^{x'} + \overline{\overline{V'}^x \delta_{y'} u}^{y'}\right)\right] + \ldots \qquad (3.82)$$

Starting from (3.74), a similar procedure would lead to the scheme

$$\frac{\partial v}{\partial t} = -\frac{1}{\overline{h}^y}\left[\frac{1}{3}\left(\overline{\overline{U}^y \delta_x v}^x + \overline{\overline{V}^y \delta_y v}^y\right) + \frac{2}{3}\left(\overline{\overline{U'}^y \delta_{x'} v}^{x'} + \overline{\overline{V'}^y \delta_{y'} v}^{y'}\right)\right] + \ldots \qquad (3.83)$$

Thus, the approximation (3.82)-(3.83) represent the E-grid advection scheme that we have been looking for.

Let us now examine the properties of the scheme (3.82)-(3.83). The conservation of momentum follows immediately from (3.79). To prove the energy conservation we shall use the identity

$$A\,\overline{B \delta_\lambda A}^\lambda = -\frac{1}{2} A^2 \delta_\lambda B + \delta_\lambda\left(B \tfrac{1}{2} \widetilde{AA}^\lambda\right) , \qquad (3.84)$$

where the symbol $\widetilde{AA}^\lambda$ denotes the product of the values of the variable A at two neighbouring grid points located on a coordinate line oriented in the direction of the coordinate axis λ. Multiplying (3.82) by $\overline{h}^x u$,

with the aid of (3.84) we find that

$$\overline{h}^{x}\frac{\partial}{\partial t}\tfrac{1}{2}u^{2}=\tfrac{1}{2}u^{2}\overline{\left[\tfrac{1}{3}(\delta_{x}U+\delta_{y}V)+\tfrac{2}{3}(\delta_{x'}U'+\delta_{y'}V')\right]}^{x}$$
$$-\left\{\tfrac{1}{3}\left[\delta_{x}(\overline{U}^{x}\tfrac{1}{2}\widetilde{uu}^{x})+\delta_{y}(\overline{V}^{x}\tfrac{1}{2}\widetilde{uu}^{y})\right]+\tfrac{2}{3}\left[\delta_{x'}(\overline{U'}^{x}\tfrac{1}{2}\widetilde{uu}^{x'})+\delta_{y'}(\overline{V'}^{x}\tfrac{1}{2}\widetilde{uu}^{y'})\right]\right\}+\ldots \tag{3.85}$$

However, taking into account the continuity equation (3.81), (3.85) may be rewritten in the form

$$\frac{\partial}{\partial t}(\overline{h}^{x}\tfrac{1}{2}u^{2})=-\left\{\tfrac{1}{3}\left[\delta_{x}(\overline{U}^{x}\tfrac{1}{2}\widetilde{uu}^{x})+\delta_{y}(\overline{V}^{x}\tfrac{1}{2}\widetilde{uu}^{y})\right]\right.$$
$$\left.+\tfrac{2}{3}\left[\delta_{x'}(\overline{U'}^{x}\tfrac{1}{2}\widetilde{uu}^{x'})+\delta_{y'}(\overline{V'}^{x}\tfrac{1}{2}\widetilde{uu}^{y'})\right]\right\}+\ldots \tag{3.86}$$

When the summation is performed over a closed domain, or a domain with cyclic boundary conditions, the contribution of the right hand side of (3.86) vanishes, and therefore, the advection scheme (3.82) does not allow false generation of $\overline{h}^{x}\frac{1}{2}u^{2}$. Similarly, from (3.83) we find that there can be no false generation of $\overline{h}^{y}\frac{1}{2}v^{2}$ either. Thus, the scheme (3.82)-(3.83) is indeed energy conserving.

d. Experimental results

In order to illustrate the effect of different definitions of the "eigenvalues" (3.54) and (3.75) in long term integrations, we shall here reproduce some experimental results of Janjić (1984).

In his experiments, the shallow water equations were integrated in a square domain with constant Coriolis parameter. The mirror image boundary conditions were specified. Physically, this experiment design corresponds to a "rotating flat square earth" with the solution on one side being the mirror image of the solution on the other.

In the main experiment the advection scheme (3.82)-(3.83) was applied. In the control experiment, this advection scheme was replaced by the scheme obtained by exchanging places of the averaging operators with respect to x and y applied to the mass fluxes appearing in (3.82)-(3.83). In the case of non-divergent flow, the scheme obtained in this manner reduces to the scheme (3.46)-(3.47) which conserves energy and enstrophy as defined on the E grid. Except for the advection terms,

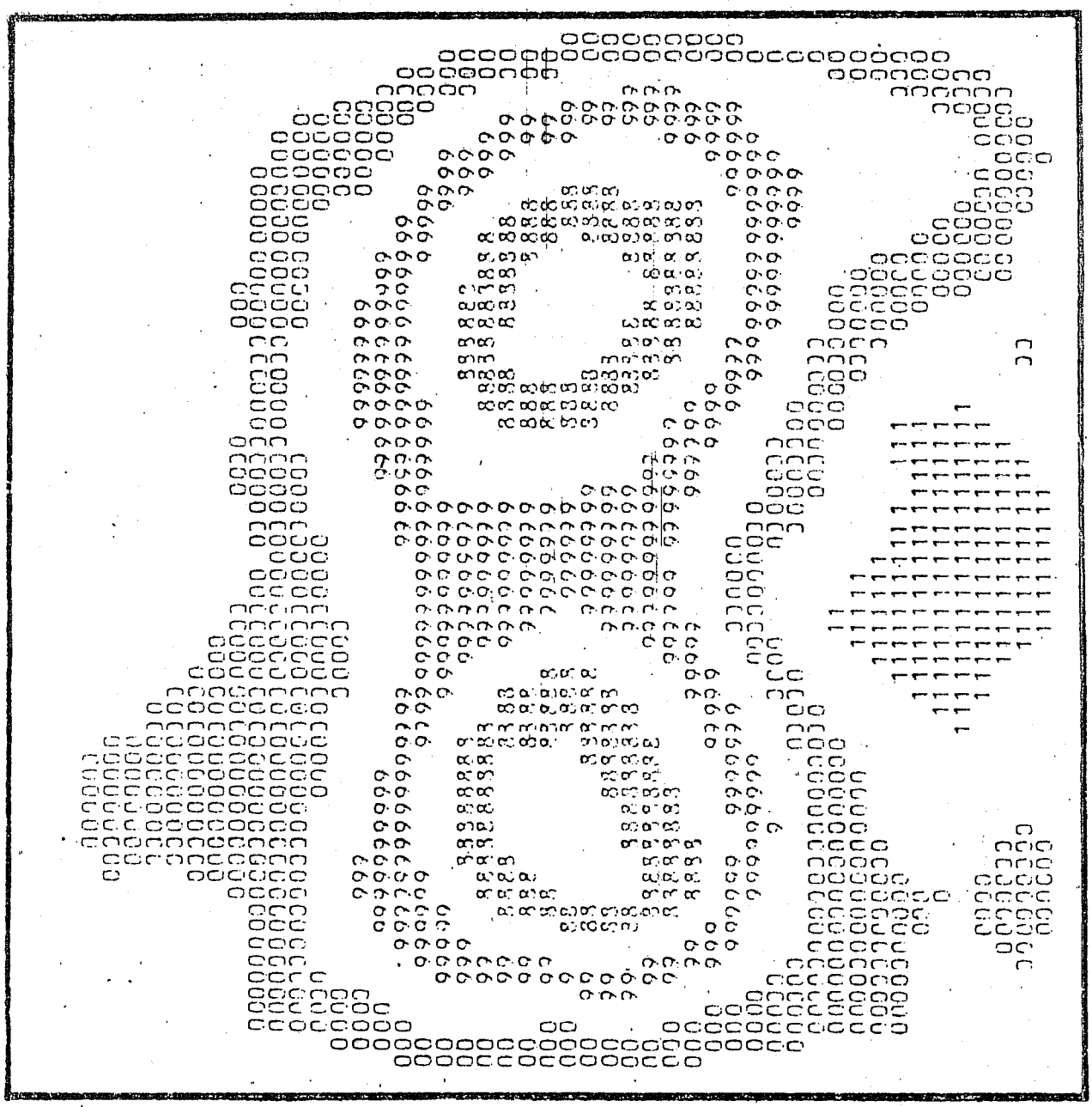

Fig. 3.9. Height field after 10000 time steps in the main experiment. The shading interval is 160 m. (After Janjić, 1984)

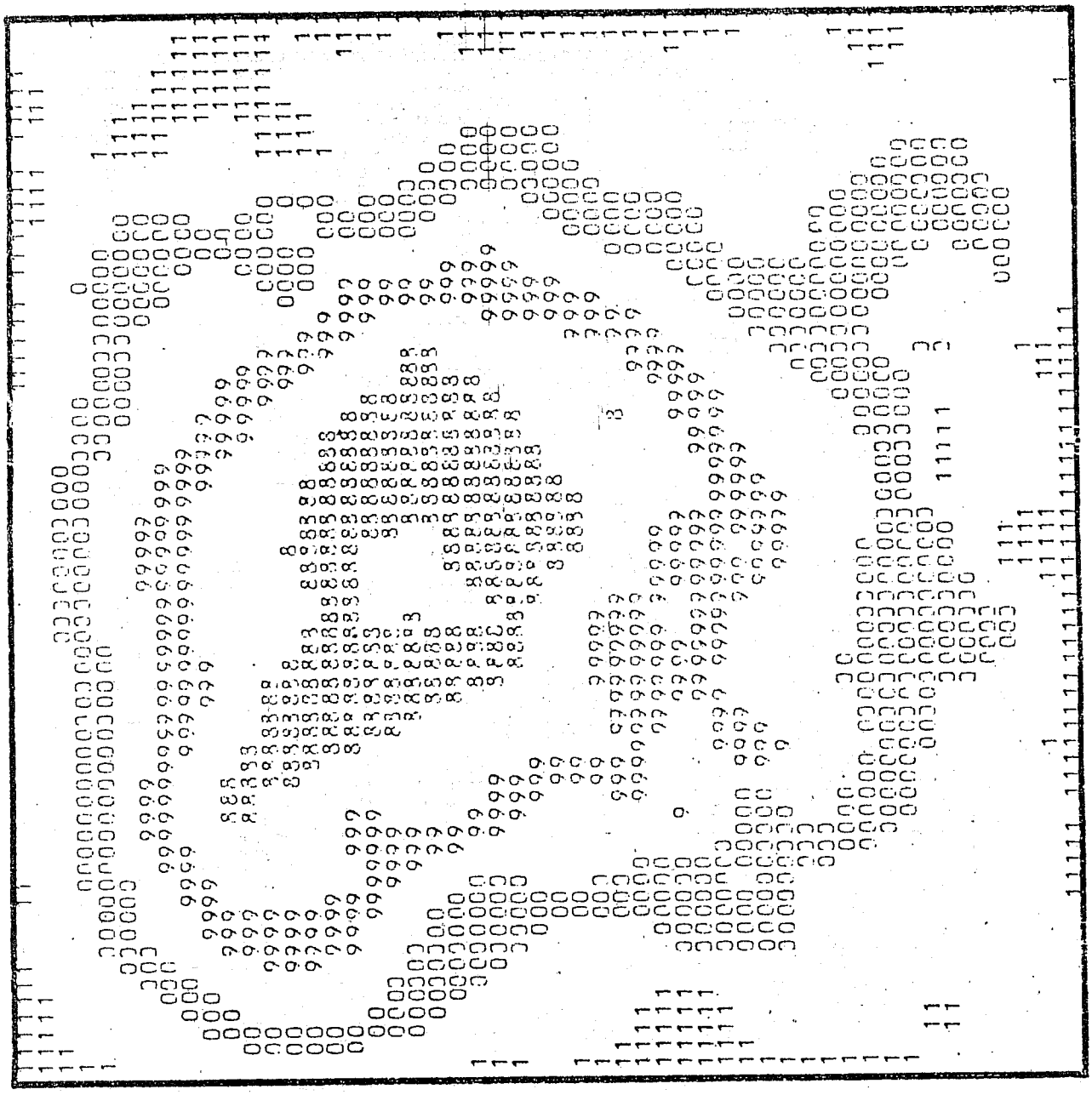

Fig. 3.10. Height field after 10000 time steps in the control experiment. The shading interval is 160 m. (After Janjić, 1984)

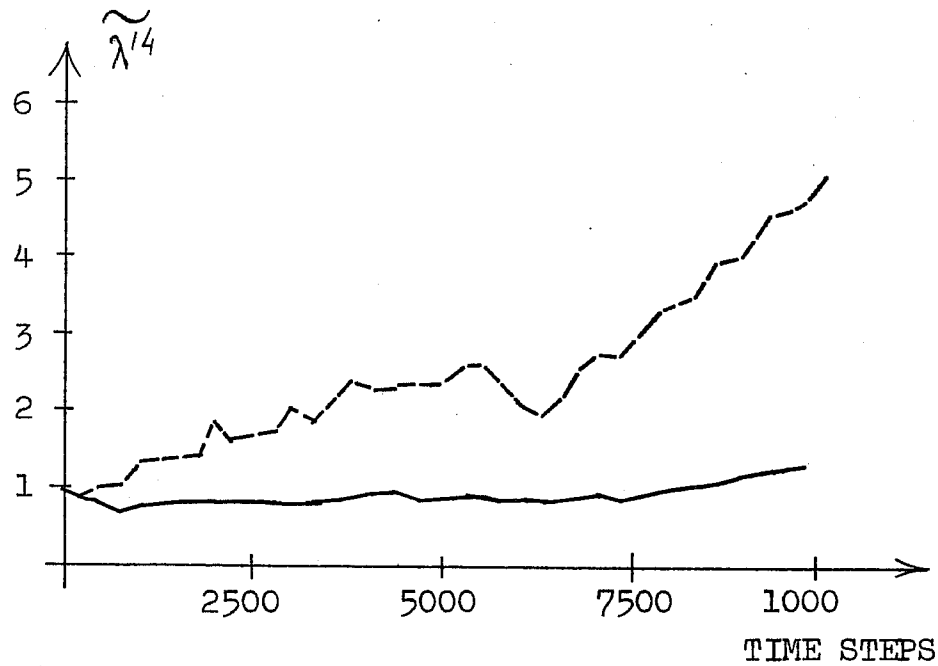

Fig. 3.11. Evolution over 10000 time steps of the ratio of space averaged $\frac{1}{2}(\nabla_x^2 u)^2 + \frac{1}{2}(\nabla_x^2 v)^2$ and the average kinetic energy normalized by the initial value in the main (solid line) and control (dashed line) experiment. (After Janjić, 1984)

the main and the control experiment were identical.

The initial height field consisted of three wave components and the initial wind was calculated from the height field using the geostrophic relation. The leapfrog scheme with time filter was used for time integration. The experiments were terminated after 10000 time steps, or approximately 116 days.

The 10000 time steps "forecasts" of the height field obtained in the main and the control run are shown in Figs. 3.9 and 3.10 respectively. The field obtained using the scheme (3.82)-(3.83) shows well preserved wave-like structure, although energy is shifted towards larger scales as compared to the initial situation. Note that the small scale noise is almost completely absent. Presumably, the shift of energy was made possible by the loss of energy due to the damping of the gravity-inertia waves that has happened through the use of the time filter in the course of integration. On the other hand, in the control run, the energy is shifted to both large and small scales resulting in a rather noisy "zonal" flow pattern.

As another illustration, the evolution of the quantity

$$\widetilde{\lambda'^4} = \frac{\overline{\frac{1}{2}(\nabla_x^2 u)^2 + \frac{1}{2}(\nabla_x^2 v)^2}}{\overline{K}} \qquad (3.87)$$

normalized by its initial value is shown in Fig. 3.11. In (3.87) the symbol $\overline{K}$ represents the total mean kinetic energy including the divergent part. As can be easily verified, this expression has the dimension of λ'^4 and represents its weighted mean. Note that in contrast to enstrophy, $\widetilde{\lambda'^4}$ is not sensitive to the variation of the total kinetic energy. The solid and the dashed line in the figure represent the results obtained in the main and the control run, respectively. As can be seen, in the case of the E-grid energy and enstrophy conserving scheme, $\widetilde{\lambda'^4}$ shows a generally increasing trend indicating that a significant amount of kinetic energy is transported towards smaller scales. By contrast to that, in the main experiment this quantity remains close to unity, and therefore, unrealistic redistribution of kinetic energy is successfully prevented by the scheme (3.82)-(3.83).

.5 Conclusions and summary of the main results

We have examined three non-linear advection schemes. One of them as a representative of energy and enstrophy conserving schemes on the staggered grid C, while the other two were defined on the semi-staggered grid E.

It has been demonstrated that due to different definitions of rotational wind and vorticity, the conservation of energy and enstrophy in the two grids does not have the same meaning. In contrast to the grid C, on the E grid these constraints do not guarantee that the transport of energy towards smaller scales will be limited.

However, using a new approach to the application of the Arakawa Jacobian, Janjić (1984) derived an E grid scheme which exactly reflects the Arakawa theory for the non-divergent flow. This was achieved by conservation of energy and enstrophy as defined on the C grid. These two quantities cannot be calculated directly from the dependent variables on the E grid, and thus, in a way, may be considered to belong to the sub-grid scales. It has been demonstrated that the amount of energy which can be transported towards smaller scales is more restricted than for any other scheme of this type on both C and E grids.

In order to summarize the properties of the schemes with respect to the simulation of the non-linear energy cascade, it is convenient to use the mechanical analogy of Charney (e.g. Mesinger and Arakawa, 1976). For this purpose, we shall introduce the "average wave-number squared" which is defined by the ratio of enstrophy and energy. Thus, for the E-grid scheme (3.23)-(3.24), we have

$$\overline{\lambda'^2} = \frac{\eta'}{K'} = \frac{\sum_{p}^{P} \lambda_p'^2 K_p'}{\sum_{p}^{P} K_p'} \quad . \tag{3.88}$$

Similarly, for the schemes (3.46)-(3.47) and (3.73)-(3.74) we obtain, respectively,

$$\overline{\lambda^2} = \frac{\eta}{K} \quad \frac{\sum_{p}^{P-1} \lambda_p^2 K_p}{\sum_{p}^{P-1} K_p} \quad , \tag{3.89}$$

$$\overline{\Lambda^2} = \frac{\eta'}{K} \quad \frac{\sum_{p}^{P-1} \Lambda_p^2 K_p}{\sum_{p}^{P-1} K_p} \quad . \tag{3.90}$$

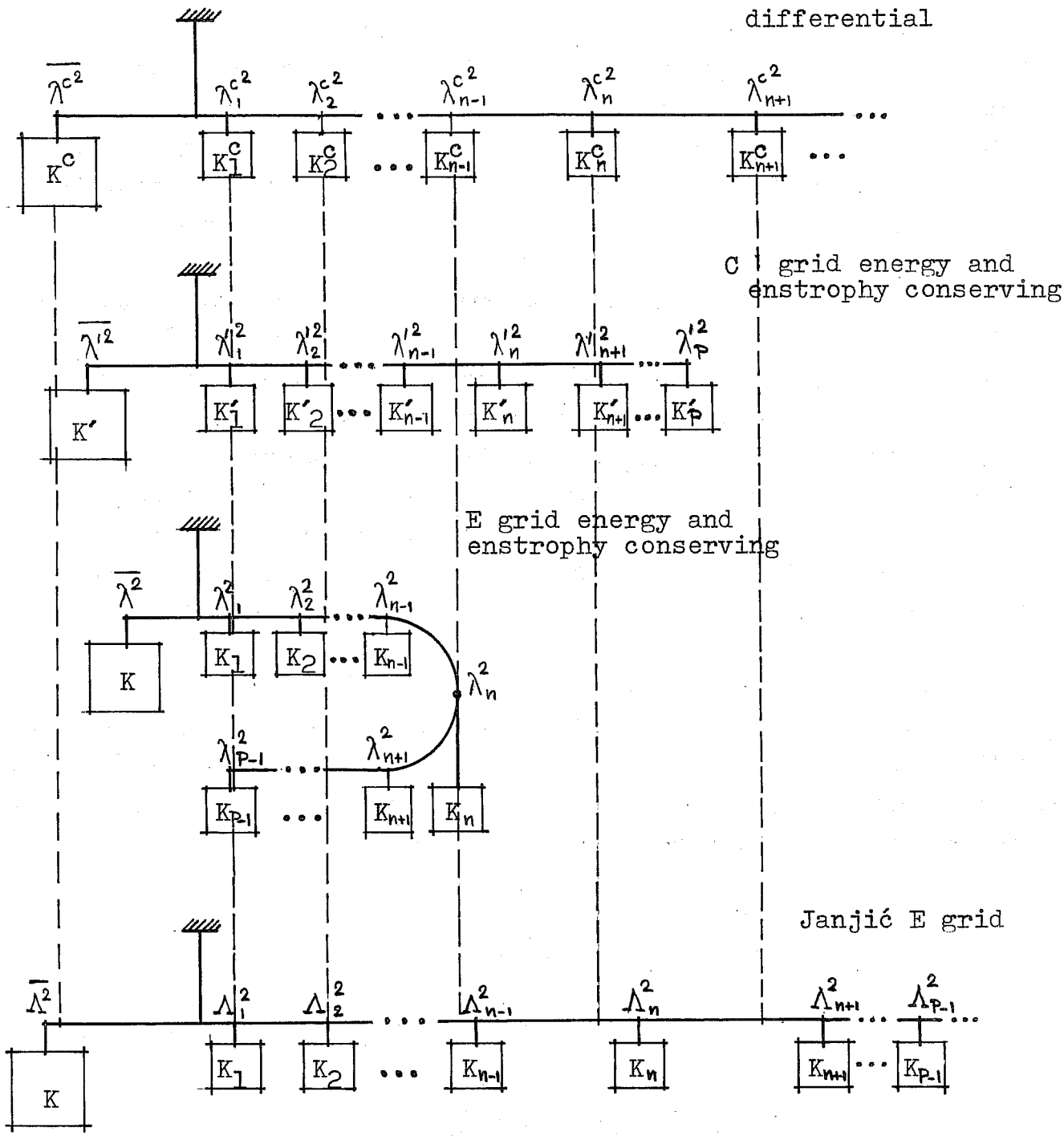

Fig. 3.12. Mechanical analogies of the constraints imposed on the non-linear energy cascade in the continuous case, in the case of the C-grid energy and enstrophy conserving scheme, in the case of the E-grid energy and enstrophy conserving scheme, and in the case of the scheme due to Janjić (1984).

Here, K', η', K and η are defined by (3.43), (3.44), (3.61) and (3.62). The relations (3.88)-(3.90) can now be rewritten in the form

$$\overline{\lambda'^2}\, K' = \sum_{p}^{P} \lambda'^2_p K'_p \,, \tag{3.91}$$

$$\overline{\lambda^2}\, K = \sum_{p}^{P-1} \lambda^2_p K_p \,, \tag{3.92}$$

$$\overline{\Lambda^2}\, K = \sum_{p}^{P-1} \Lambda^2_p K_p \,. \tag{3.93}$$

Of course, an analogous relation is valid for the continuous case (e.g. Mesinger and Arakawa, 1976).

Let us now imagine a suspended weightless rod representing an ideal balance. Let a weight equal to the mean kinetic energy be suspended to the left of the point of suspension of the rod, at a distance equal to the mean wave-number squared, and let the weights equal to the kinetic energies associated with each eigenvalue be suspended on the right hand of the balance at the distances equal to the corresponding eigenvalues. The relations of the form (3.91)-(3.93) then can be considered as the requirements for mechanical equilibrium of such a system. Such mechanical analogies for the continuous case and the three considered schemes are schematically represented in Fig. 3.12. The superscript c denotes the quantities corresponding to the continuous case. The interchange of mass between the weights on the right hand sides of the balances is permitted, but only in such a way as to maintain the equilibrium. As compared to the continuous case, the "distances" λ'^2_p corresponding to the C grid are shorter, more and more so as the smallest resolvable scale is approached; and the right hand of the balance is of limited extension. Thus, if initially there is little energy in the shortest scales, as normally would be the case, a subsequent false energy cascade into the shortest scales will not be as strongly restricted as it should according to the continuous equations. Considering the E-grid energy and enstrophy conserving scheme, the fact that the eigenvalues λ^2_p are not monotonically increasing with increasing the wave-number is schematically represented in the figure by bending the right hand of the balance. Apparently, in this situation, relatively weak constraints on the exchange of energy among the modes are imposed. Finally, in the case of the Janjić (1984) E-grid scheme, the distances Λ^2_p are longer than those of the continuous case, and very much longer

for the shortest scales, with the "eigenvalues" tending to infinity as the shortest resolvable scale is approached. Thus, if again we consider the situation where initially very little energy is present in the shortest scales, a subsequent systematic energy cascade into these scales will be even more restricted than with the continuous equations. The shortest resolvable scale is moved to infinity, in some resemblance to shortest, infinitely small, scale of the continuous case.

Acknowledgements

The preparation of this manuscript was partly supported by the Science Association of Serbia.

The authors are grateful to mr. M. Stambolić for highly efficient drawing of the figures.

REFERENCES

Arakawa, A., 1966: Computational design for long term numerical integration of the equations of fluid motion: Two-dimensional incompressible flow. Part I. J. Comput. Phys., 1, 119-143.

_____, 1972: Design of the UCLA general circulation model. Dept. of Meteorology, Univ. of California, Los Angeles, Numerical Simulation of Weather and Climate, Tech. Rept. No. 7, 116 pp. (Available from the Department of Atmospheric Sciences, University of California at Los Angeles, Calif. 90024)

_____ and V.R. Lamb, 1977: Computational Design of the Basic Dynamical Processes of the UCLA General Circulation Model. Methods in Computational Physiscs, Academic Press, New York, 173-265.

_____ and _____, 1981: A potential enstrophy and energy conserving scheme for the shallow water equations. Mon. Wea. Rev., 109, 18-36.

Basdevant, C., and R. Sadourny, 1975: Ergodic properties of inviscid truncated models of two-dimensional incompressible flows. J. Fluid Mech., 69, 673-688.

Bates, J.R., 1984a: An efficient semi-Lagrangian and alternating direction implicit method for integrating the shallow water equations. (Submitted to Mon. Wea. Rev.)

_____, 1984b: Semi-Lagrangian advective schemes and their use in meteorological modeling. AMS-SIAM 1983 Summer Seminar: Large-Scale Computations in Fluid Mechanics. Scripps Institution of Oceanography, La Jolla, California, American Mathematical Society. (To appear in Lectures in Applied Mathematics, 22)

_____ and A. McDonald, 1982: Multiply-upstream semi-Lagrangian advective schemes: analysis and application to a multi-level primitive equation model. Mon. Wea. Rev., 110, 1831-1842.

Burridge, D.M. and J. Haseler, 1977: A model for medium range weather forecasting - adiabatic formulation. European Centre for Medium Range Weather Forecasts, Tech. Rept. No. 4, 46 pp. (Available from the European Centre for Medium Range Weather Forecasts, Shinfield Park, Reading, Berks. RG2 9AX, UK)

Fjørtoft, R., 1953: On the changes in spectral distribution of kinetic energy for two-dimensional, nondivergent flow. Tellus, 5, 225-230.

Gadd, A.J., 1974: An economical explicit integration scheme. Meteorological Office Tech. Note 44, 7 pp.

_____, 1978: A split explicit integration scheme for numerical weather prediction. Quart. J. Roy. Meteor. Soc., 104, 569-582.

Gerrity, J., Jr. and R. McPherson, 1970: Noise analysis of a limited-area fine-mesh prediction model. ESSA Technical Memorandum WBTM NMC 46, NMC Washington, 81 pp.

Grammeltvedt, A., 1969: A survay of finite difference schemes for primitive equations for a barotropic fluid. Mon. Wea. Rev., 97, 384-404.

Haltiner, G.J., 1971: Numerical Weather Prediction. Wiley, New York, 317pp.

Haurwitz, B., 1943: The effect of gradual wind change on the stability of waves. Ann. N. Y. Acad. Sci., 44, 69-80.

Janjić, Z.I., 1974: A stable centered difference scheme free of two-grid -interval noise. Mon. Wea. Rev., 102, 319-323.

_____, 1977: Pressure gradient force and advection scheme used for forecasting with steep and small scale topography. Beitr. Phys. Atmosph., 50, 186-199.

_____, 1979: Forward-backward scheme modified to prevent two-grid -interval noise and its application in sigma coordinate models. Beitr. Phys. Atmosph., 52, 69-84.

_____, 1984: Non-linear advection schemes and energy cascade on semi -staggered grids. (To appear in Mon. Wea. Rev., 112)

_____ and A. Wiin-Nielsen, 1977: On geostrophic adjustment and numerical procedures in a rotating fluid. J. Atmos. Sci., 34, 297-310.

Mesinger, F., 1973: A method for construction of second-order accuracy difference schemes permitting no false two-grid-interval wave in the height field. Tellus, 25, 444-458.

_____, 1974: An economical explicit scheme which inherently prevents the false two-grid-interval wave in the forecast fields. Proceedings of the Symposium on Difference and Spectral Methods for Atmosphere and Ocean Dynamics Problems, Novosibirsk, 17-22 September 1973, Part II, 18-34.

_____, 1979: Dependence of vorticity analogue and the Rossby wave phase speed on the choice of horizontal grid. Bulletin T.LXIV de l'Academie Serbe des Sciences et des Arts. Sciences Mathématiques, No. 10, 5-15.

_____, 1981: Horizontal advection schemes of a staggered grid - an enstrophy and energy-conserving model. Mon. Wea. Rev., 109, 467-478.

_____ and A. Arakawa, 1976: Numerical methods used in atmospheric models. Vol. I. JOC, GARP Publications Series No. 17, Geneva, 64 pp. (Available from the World Meteorological Organization, CP No. 5, CH-1211, Geneva 20)

Ničković, S., 1979: The effect of horizontal differencing on the shearing instability mechanism. Beitr. Phys. Atmosph., 52, 126-135.

Sadourny, R., 1975: The dynamics of finite-difference models of the shallow-water equations. J. Atmos. Sci., 32, 680-689.

_____ and P. Morel, 1969: A finite-difference approximation of the primitive equations for a hexagonal grid on a plane. Mon. Wea. Rev., 97, 439-445.

Shapiro, R., 1970: Smoothing, filtering and boundary effects. Rev. Geophys. Space Phys., 8, 359-387.

Vasiljević, D., 1982: The effect of Mesinger's procedure for preventing grid separation on the geostrophic mode. Beitr. Phys. Atmosph., 55, 177-181.